



Identification of surface urban heat versus cool islands for arid cities depends on the choice of urban and rural definitions

Zehong Liu^a, Richen Ye^b, Qiquan Yang^{c,d,*}, Ting Hu^a, Yue Liu^e, TC Chakraborty^f, Zhenxuan Liao^g

^a School of Remote Sensing and Geomatics Engineering, Nanjing University of Information Science and Technology, Nanjing 210044, China

^b Guangzhou Urban Planning & Design Survey Research Institute Co., Guangzhou 510060, China

^c College of Surveying & Geo-Informatics, Tongji University, Shanghai 200092, China

^d State Key Laboratory of Lunar and Planetary Sciences, Macau University of Science and Technology, Macau, China

^e Guangzhou Institute of Geography, Guangdong Academy of Sciences, Guangzhou 510070, China

^f Pacific Northwest National Laboratory, Richland, WA, USA

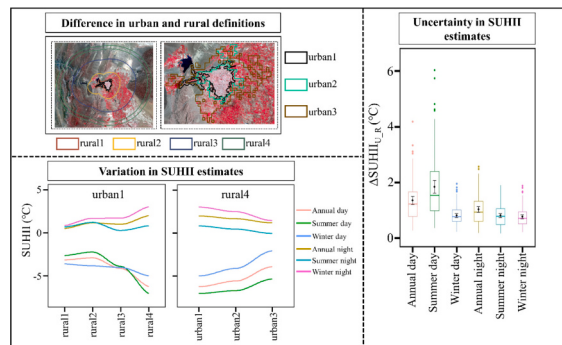
^g School of Information Engineering, Sanming University, Sanming 365004, Fujian Province, China



HIGHLIGHTS

- The estimated SUHII is largely influenced by urban and rural definitions
- Daytime SUHII shows a sign reversal in nearly half of arid cities
- The SUHII uncertainty is related to the discrepancy in the surface properties

GRAPHICAL ABSTRACT



ARTICLE INFO

Editor: Shuqing Zhao

Keywords:

Urban heat islands
Quantification methods
Arid cities
Uncertainty
Globe

ABSTRACT

The urban heat island (UHI) effect in arid cities can be small or even negative, the latter known as the urban cool island (UCI) effect. Differences in defining urban and rural areas can introduce uncertainties in detecting UHI or UCI, especially when the UHI signal is small. Here, we compared the surface UHI intensity (SUHII) estimated by a dozen different methods (with multiple urban and/or rural definitions) across 104 arid cities globally, providing a comprehensive evaluation of the uncertainty in SUHII estimates. Results show that the absolute difference in annual average SUHII (ΔSUHII) among methods exceeded 1 °C in about half of the arid cities during both daytime and nighttime. The overall annual mean ΔSUHII for all arid cities was 1.35 °C during daytime and 1.03 °C at night. The uncertainty arising from simultaneous variations in urban and rural definitions was generally higher than that resulting from their individual changes. It was observed that, with varying definitions of urban and rural areas, nearly 50 % of arid cities experienced a sign reversal in daytime SUHII estimates, while approximately 15 % exhibited a sign reversal in nighttime SUHII. Variations in urban-rural differences in surface

* Corresponding author at: College of Surveying & Geo-Informatics, Tongji University, Shanghai 200092, China.

E-mail address: qiquanyang@tongji.edu.cn (Q. Yang).

properties, such as vegetation index and albedo, due to differing urban and rural definitions, contributed strongly to the observed SUHII uncertainties. Overall, our results offer new insights into the ongoing debate on heat and cold islands in arid cities, emphasizing a critical need to standardize SUHII estimation frameworks.

1. Introduction

The process of urbanization involves changes in land cover and intensive anthropogenic activities, often resulting in local temperature increases and giving rise to the urban heat island (UHI) effect. The UHI effect has received growing attention because of its impact on urban microclimate, energy consumption, and the health of urban residents (Mavrogianni et al., 2011; Ward et al., 2016; Zhong et al., 2017). In recent years, with the development of remote sensing technology, satellite-derived land surface temperature (LST) has been widely used to estimate the surface UHI (SUHI) effect. Existing studies have comprehensively analyzed the SUHI effect from various aspects, including quantification methods (Liu et al., 2023; Chakraborty et al., 2021; Yang et al., 2023b; Li et al., 2019), spatiotemporal variations (Chakraborty and Lee, 2019; Li et al., 2019; Wang et al., 2015; Siddiqui et al., 2021), driving factors (Li et al., 2020a; Geng et al., 2023; Zhou et al., 2014), and potential impacts (Luo and Asproudi, 2015; Dihkan et al., 2015). Accurate quantification of the SUHI effect is of fundamental importance for better constraining its variability and impacts.

The SUHI intensity (SUHII) is the quantitative magnitude of this effect, and is typically defined as the average difference in LST between urban and rural areas. The prerequisite for accurate estimation of SUHII thus relies on the delineation of urban and rural areas. Numerous methods have been developed to quantify SUHII, with differences in the definitions of urban and rural areas (Table 1). These differences can lead to discrepancies in the mean LST with urban and rural areas, thereby altering the quantified SUHII values. Multiple studies have focused on the influence of rural definition on the estimation of SUHII (Schwarz et al., 2011; Yao et al., 2018; Li et al., 2019; Li et al., 2022; Yang et al., 2023b; Liu et al., 2023). For example, Yao et al. (2018) and Li et al. (2022) found that using the rural area near the urban area would underestimate SUHII in summer daytime, and it was more advisable to use rural areas far away from the urban area for estimating SUHII. Li et al. (2019) and Yang et al. (2023b) found that SUHII varied greatly along the urban-rural gradients, especially during the daytime, and the difference in rural definition led to large uncertainties in estimated SUHII. Liu et al. (2023) found that the magnitude and direction of the SUHII trend were significantly influenced by the selection of various rural references. In addition to the rural area, the variability in urban area can also pose a non-negligible impact on SUHII estimations given that changes in urban extent can directly alter its inner mean LST (Yang et al., 2023a). Currently, there are numerous publicly available products delineating global urban areas, and several (e.g., the Moderate Resolution Imaging Spectroradiometer (MODIS) land cover product) have been widely used in SUHI-related studies (Chakraborty and Lee, 2019; Du et al., 2021; Hu et al., 2022; Tuholske et al., 2021; Liu et al., 2022a; Yao et al., 2019). However, inconsistencies persist among current urban products due to differences in data sources and extraction methods (Yang et al., 2023a). In summary, current studies exhibit variations in the definition of urban and rural areas, introducing potential uncertainties in quantifying the SUHI effect. However, there is still a gap in large-scale studies that synthesize the combined effects of urban and rural definitions on SUHI estimates.

The SUHII in arid cities has always shown atypical signals, and thus has attracted great interest from researchers (Gaur and Squires, 2018; Shen and Chen, 2010; Dialesandro et al., 2019; Abulibdeh, 2021; Bakarman and Chang, 2015). Existing research has not yet reached a consensus on the spatial distribution, magnitude, and temporal pattern of SUHII in arid cities, particularly for daytime (Zhang et al., 2022; Shafieyou et al., 2023; Rasul et al., 2016; Mohammad et al., 2019).

Many studies have indicated that urban areas in arid cities often display lower temperatures compared to its peripheral areas, a phenomenon characterized as the urban cold island (UCI) effect (e.g., Li and Chen, 2023; Rasul et al., 2017; Mohammad and Goswami, 2021; Lazzarini et al., 2015). Nonetheless, other large-scale satellite-based estimates have shown small but positive SUHII in arid zones (Chakraborty and Lee, 2019; Chakraborty et al., 2020). Even for the same city (e.g., Isfahan, Iran), there may be different conclusions regarding the magnitude of the UHI (Shirani-Bidabadi et al., 2019) or UCI (Zandi, R, et al., 2023). This study hypothesizes that this ongoing controversy may be related to the uncertainty caused by the estimation method, especially the delineation method of urban and rural boundaries. Arid cities are surrounded not only by typical desert vegetation but also by barren areas which have very different LST (Campos and Brito, 2018; Wang et al., 2021; Liu et al., 2021). Changing the urban-rural extent can alter their inner land cover composition and LST, thereby increasing the spatial variability and sensitivity of SUHII. Hitherto, there is still a lack of large-scale quantitative analyses regarding the influence of urban and rural definitions on identifying the UHI and UCI for arid cities.

Here, we select 104 cities across global arid regions and estimate their SUHII using 12 distinct methods with distinct urban and rural definitions. The absolute difference in SUHII (Δ SUHII) among these methods is considered as the potential SUHII uncertainty induced by urban and rural definitions. We conduct a comprehensive analysis of the spatial and temporal patterns of Δ SUHII across arid cities globally. The purpose of this study is to: (1) explore the impact of quantification methods on SUHII estimates integrating both urban and rural definitions; and (2) contribute to the ongoing debate regarding heat and cold islands in arid cities.

2. Data

2.1. Global urban area data

Three widely used datasets, including the Global Urban Boundary (GUB) dataset, the Global Human Settlement Layer (GHSL) dataset, and a MODIS land cover product (MCD12Q1, shorted as MCD), were used for delineating urban area in this study. The GUB and MCD data were obtained from 2018, while the GHSL data were derived from 2020, the closest available year to the other two data. These datasets enabled the extraction of global coverage for urban areas and have been employed in numerous studies related to the SUHI effect. The urban areas delineated by different datasets vary greatly (Yang et al., 2023a), providing a valuable opportunity for analyzing the uncertainty in SUHII induced by urban area definitions. Details of these datasets are provided below.

The extraction of the GUB relied on the 30-m resolution global artificial impervious area product released by Gong et al. (2020). These data were first converted into a kernel density map using a kernel density estimation method. Pixels with kernel density values exceeding 20 % were categorized as urban pixels. Subsequently, the urban pixels were transformed into vectors and subjected to additional processing through morphological operations to define the boundaries of the urban area (Li et al., 2020b). The GUB has shown advantages in spatial resolution and has been widely used in recent SUHI studies (e.g., Du et al., 2021; Hu et al., 2022; Liu et al., 2022b; Yang et al., 2021).

The delineation of the GHSL urban area involved identifying a concentrated grouping of spatially generalized adjacent grid squares (Florczyk et al., 2019). This grouping should have an area of 1 km², a population density of no <1500 inhabitants per km², or at least 50 % of the built-up surface covered per km² of surface, along with a requisite

Table 1

A summary of classical methods for estimating the SUHII.

Methods	Descriptions	Strength & Weakness	Indicators	References
Distance-based methods	The difference in mean LST between the urban area and the ring buffer with a specific width at a certain distance from the urban area	Distance-based methods have the advantages of simple construction and efficient buffer creation, but they are constrained by the inability to apply a single fixed buffer to cities of varying sizes (Lai et al., 2018)	Urban areas are identified using the MODIS land cover product, while rural areas are defined as a 20 km wide ring buffer starting 10 km from the urban area. Urban areas are defined as regions with a high density of impervious surfaces, while rural areas are defined as a 5 km ring buffer starting 45 km from the urban area. Urban areas are extracted from the Global Human Settlement Layer (GHSL) dataset, while rural areas are defined as a 10 km ring buffer adjacent the urban area. Urban areas are extracted from the Landscan population dataset, while rural areas are defined as a 10 km ring buffer adjacent the urban area.	Yao et al., 2019 Imhoff et al., 2010 Venter et al., 2021 Clinton and Gong, 2013
Area-based methods	The difference in mean LST between the urban area and the nearby buffer area of several times the size of the urban area.	Area-based methods consider the size of the urban area when selecting the rural area, making them more suitable for SUHII analysis across different cities. However, they may underestimate SUHII due to the close proximity of rural areas to urban areas (Li et al., 2022).	Urban areas are identified by the MODIS land cover product, while rural areas are defined as an equal-sized buffer adjacent to the urban area. Urban areas are defined as regions with a high density of impervious surfaces,	Peng et al., 2012; Liu et al., 2022b Yang et al., 2017; Zhou et al., 2014

Table 1 (continued)

Methods	Descriptions	Strength & Weakness	Indicators	References
		Yang et al., 2023b).	while rural areas are defined as an equal-sized buffer adjacent to the urban area.	
		Landcover-based methods	The difference in mean LST between the urban area and other land cover types	Urban areas are defined as urban and built-up pixels derived from the MODIS land cover product, and rural areas are defined as all other land covers.
		Gaussian model-based methods	The maximum of a Gaussian surface fitted to the LST signal after subtracting the background	Urban and rural areas are identified by the landcover data provided by USGS EROS data center (Sellers et al., 1996).
				Urban and rural areas are identified by the MODIS land cover product.
				Streutker, 2002
				Jin et al., 2005
				Chen et al., 2006
				Tran et al., 2006

population of at least 50,000 (Florczyk et al., 2019). The GHSL dataset includes >10,000 global urban centers with a spatial resolution of 1 km, providing important data for large-scale studies on the SUHI effect (Tuholske et al., 2021; Venter et al., 2021).

The MCD was obtained through a decision tree classification with a supervised learning approach, containing five different land cover

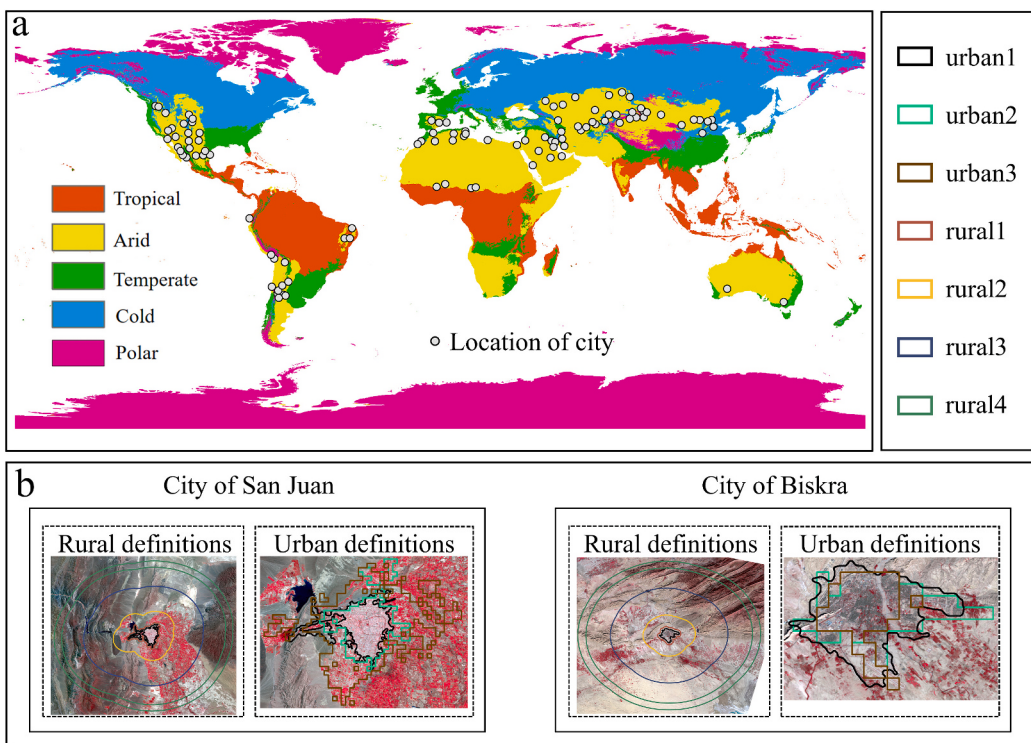


Fig. 1. (a) The spatial distribution of 104 arid cities. (b) The spatial disparity in both urban and rural areas under different definitions, taking two cities as examples. The background images of the two cities are standard false-color (R: Band 4, G: Band 3, B: Band 2) composites of Landsat data (Landsat 8–9 OLI/TIRS C2 L1).

classification schemes (Sulla-Menashe and Friedl, 2018). In this study, the categorization stemmed from the International Geosphere-Biosphere Programme (IGBP) framework that encompassed a total of 17 distinct land cover categories. The classification labeled as “Urban and Built-up Lands” was used to delineate urban areas (Sulla-Menashe and Friedl, 2018). The MCD product offers long-term year-by-year global extent of urban areas with a spatial resolution of 500 m, and has been a crucial data source for SUHI-related studies (e.g., Chakraborty and Lee, 2019; Clinton and Gong, 2013; Liao et al., 2022; Liu et al., 2022a; Peng et al., 2012; Yao et al., 2019).

2.2. LST data

This study utilized LST data from the MODIS version-6 LST product (MYD11A1) in 2018. This product provides global daily pixel-by-pixel LST with a spatial resolution of 1 km. Both daytime (approximately 13:30 local time) and nighttime (approximately 1:30 local time) LST observations are available. Previous studies have demonstrated the overall high accuracy and good applicability of the MODIS LST product (Duan et al., 2018; Wan, 2014), which has been a foundational dataset for investigating the SUHI effect (Zhou et al., 2018). Referring to previous studies (Chakraborty and Lee, 2019; Li et al., 2019; Yao et al., 2018), we excluded LST pixels with errors higher than 3 °C based on the quality assessment layer. The daily LST observations were then averaged annually and seasonally. For cities in the northern (southern) hemisphere, the periods of summer and winter were defined as June–August (December–February) and December–February (June–August), respectively.

2.3. Auxiliary data

The Global 30 Arc-Second Elevation (GTOPO30) can provide a global digital elevation model at a spatial resolution of approximately 1 km. It was developed by the United States Geological Survey in collaboration with many research institutes worldwide (Miliareis and

Argialas, 1999). This data was obtained from 2018 and was used to remove or reduce the influence of topographic relief on SUHII estimates.

The Global Surface Water (GSW) data can provide the maximum water extent across global surface with a spatial resolution of 30 m. The GSW data has a good level of accuracy, with errors of omission <5 % and commission <1 % (Pekel et al., 2016). This data was derived from 2018 and was employed to mitigate the influence of water bodies on SUHII estimates.

The global impervious surface area was provided by Huang et al. (2022), which had a spatial resolution of 30 m and an F1-score score of 0.935. We used this product for the year 2018, and calculated the impervious surface fraction (ISF) within the spatial grid corresponding to each MODIS pixel. The resultant ISF map was used to remove the influence of surrounding impervious surface area on SUHII estimates.

The Köppen climate classification map counts among the most widely used climate classification systems, dividing the global terrestrial surface into five major climate groups: tropical, arid, temperate, cold, polar zones (Kottek et al., 2006). This study used the Köppen-Geiger climate classification map with a resolution of 1 km published by Beck et al. (2018). This data was utilized to ascertain whether a city belongs to the arid climate zone.

The land cover data was obtained from the Copernicus Global Land Service (2018): CGLS-LC100 Collection 3. It has a spatial resolution of 100 m and an accuracy of 80 % (Buchhorn et al., 2020) and includes fractional estimates for basic land cover classes (built-ups, bare areas, trees, shrubs, water bodies and herbaceous, etc.). This dataset was used to discuss the spatial variations of land cover difference caused by urban and rural definitions and its possible effect on the LST.

The enhanced vegetation index (EVI) data was derived from the MODIS vegetation index product (MYD13A2). This data has a spatial resolution of 1 km and has been collected for the year 2018. The EVI is known for effectively reflecting surface vegetation and has been widely used in SUHII-related studies (Peng et al., 2012; Yang and Zhao, 2023; Yang et al., 2019; Yao et al., 2019; Zhou et al., 2014). This EVI data was used to discuss the possible reasons for the SUHII uncertainties caused

by urban and rural definitions.

The white-sky albedo (WSA) dataset was obtained from the MODIS albedo product (MCD43A3) for the year 2018. The bias of the MODIS albedo product has been reported to be mostly less 5 % (Liu et al., 2009). This product provides white-sky and black-sky albedos over shortwave broadband with a spatial resolution of 500 m. We used WSA in this study due to the strong linear association between these two types of short-wave albedos (Peng et al., 2012). The WSA data was also used to discuss the possible reasons for the SUHII uncertainties caused by urban and rural definitions.

3. Methods

The primary goal of this study is to examine how urban and rural definitions impact SUHII estimates across global arid cities. This objective can be achieved by comparing estimated SUHIIs based on different methods that vary in urban and/or rural definitions. Hence, our analysis encompasses two main steps: the delineation of urban and rural areas and the subsequent calculation and comparison of SUHII.

3.1. Delineation of urban and rural areas

The urban area for each city was delineated by using different global urban datasets, including GUB, GHSL, and MCD (refer to the section 2.1 for specific details). First, we extracted all GUB polygons situated in the arid climate zone, and merged those that were in close proximity (<2 km) to each other. The threshold of 2 km is determined based on previous studies (Lai et al., 2021; Yang and Zhao, 2023; Zhao et al., 2016; Zhou et al., 2014; Yang et al., 2023b). The same approach was also used from the GHSL polygons and MCD polygons following raster-to-vector conversion. Then, urban areas were identified based on the above merged polygons (i.e., GUB, GHSL and MCD), with the following criteria: (1) The selected urban patches exhibit overlapping regions in all three datasets; (2) The selected urban patches are larger than 20 km^2 in all three datasets. We considered polygons in each dataset that meet the above criteria as the corresponding urban areas (Fig. S1). Finally, 104 cities were selected, distributed across the global arid zone (Fig. 1). The use of a 20 km^2 threshold in this study is an empirical trade-off. Urban areas extracted from different global datasets can vary substantially, and using a higher threshold would exclude some major arid cities, reducing the number of available city samples. Conversely, a lower threshold increases the number of samples but introduces problems such as increased data uncertainty and complicated data processing. For convenience, we denote the urban areas corresponding to GUB, GHSL, and MCD as urban1, urban2, and urban3, respectively.

Rural areas can be defined in various ways, primarily categorized into area-based and distance-based methods (Table 1). The most common area-based method is to define the rural area as an equal-sized buffer adjacent to its central urban area (Yang et al., 2023b; Li et al., 2019; Chakraborty et al., 2021). This study incorporated such an area-based method, and the rural area obtained through this method was referred to as “rural1”. The distance-based method generally defined a ring buffer with a specific width (w) at a certain distance (d) from the urban area as the rural area (Clinton and Gong, 2013; Yang et al., 2023b). The selection of d and w varied among studies, and this study incorporated three classical assignments for d and w : (1) $d = 0$, $w = 10 \text{ km}$ (Clinton and Gong, 2013); (2) $d = 10 \text{ km}$, $w = 20 \text{ km}$ (Yao et al., 2019); (3) $d = 45 \text{ km}$, $w = 5 \text{ km}$ (Imhoff et al., 2010). The rural areas corresponding to the three combinations of d and w were labeled as “rural2”, “rural3”, and “rural4”, respectively. To mitigate the influence of confounding factors, we excluded specific regions within the rural areas based on the following conditions: (1) regions covered by water bodies; (2) regions influenced by elevation anomalies (deviating from urban median elevation by 50 m); (3) regions covered by other urban pixels; and (4) regions affected by impervious surfaces (ISF > 5 %). We applied a stringent threshold of 5 %, as it is the most commonly used

Table 2

Descriptions of urban and rural definitions used in this study.

	Description	Reference
urban1	The urban area derived from the Global Urban Boundary (GUB) dataset	Gong et al., 2020; Li et al., 2020b
urban2	The urban area obtained from the Global Human Settlement Layer (GHSL) dataset	Florczyk et al., 2019
urban3	The urban area obtained from the MODIS land cover product (MCD12Q1)	Sulla-Menashe and Friedl, 2018
rural1	The rural area is defined as an equal-sized buffer adjacent to its central urban area	Yang et al., 2023b; Li et al., 2019
rural2	The rural area is defined as a ring buffer with a specific width (w) at a certain distance (d) from the urban area as the rural area ($d = 0$, $w = 10 \text{ km}$)	Clinton and Gong, 2013
rural3	$d = 10 \text{ km}$, $w = 20 \text{ km}$	Yao et al., 2019
rural4	$d = 45 \text{ km}$, $w = 5 \text{ km}$	Imhoff et al., 2010

threshold (Imhoff et al., 2010; Yao et al., 2018; Yang et al., 2023a). This processing helps ensure that the rural areas are more representative of the natural background climate.

3.2. Calculation and comparison of SUHII estimates

This study incorporated three types of urban definitions (urban1, urban2, and urban3) and four types of rural definitions (rural1, rural2, rural3, and rural4) (Table 2). Thus, in each city, there were 12 (i.e., 3×4) different methods for estimating SUHII, with variations in urban and rural definitions. For a given city, assuming that the mean LST of the i th ($i = 1, 2$, or 3) urban area is $LST_{u,i}$, and the mean LST of the j th ($i = 1, 2, 3$, or 4) rural area is $LST_{r,j}$. Then, the corresponding SUHII can be expressed as:

$$SUHII_{ij} = LST_{u,i} - LST_{r,j} \quad (1)$$

Obviously, for each city, there were 12 different SUHII estimates derived from various combinations of urban and rural areas. Then, we performed the following comparative analysis:

(1) Comparing SUHII estimates with varying rural definitions while keeping the urban definition constant. For example, by fixing the urban area as urban1, we made a paired comparison of SUHII estimates (i.e., $SUHII_{11}$, $SUHII_{12}$, $SUHII_{13}$, and $SUHII_{14}$) for four different rural areas (i.e., rural1, rural2, rural3, and rural4). The absolute difference between these SUHII estimates reflects the uncertainty caused by rural definitions.

(2) Comparing SUHII estimates with varying urban definitions while keeping the rural definition constant. For example, by fixing the rural area as rural1, we made a paired comparison of SUHII estimates (i.e., $SUHII_{11}$, $SUHII_{21}$, $SUHII_{31}$) for three different urban areas (i.e., urban1, urban2, urban3). The absolute difference between these SUHII estimates reflects the uncertainty caused by urban definitions.

(3) Comparing SUHII estimates for all combinations of urban and rural definitions. The absolute difference between these SUHII estimates reflects the uncertainty caused by co-variation of urban and rural definitions.

4. Results

4.1. Variations in SUHII estimates arising from different urban and/or rural definitions

As shown in Figs. 2–3 and Table 3, arid cities experienced high variability in SUHII estimates when based on different urban and/or rural definitions. For instance, the annual daytime SUHII reached its highest average value ($0.19 \pm 0.44 \text{ }^\circ\text{C}$) when determined by urban3 & rural1 (i.e., $SUHII_{31}$) and showed the lowest average value ($-1.10 \pm 0.61 \text{ }^\circ\text{C}$) when derived from urban2 & rural4 (i.e., $SUHII_{24}$). Notably, nearly 30 % of arid cities exhibited sign changes in SUHII estimates

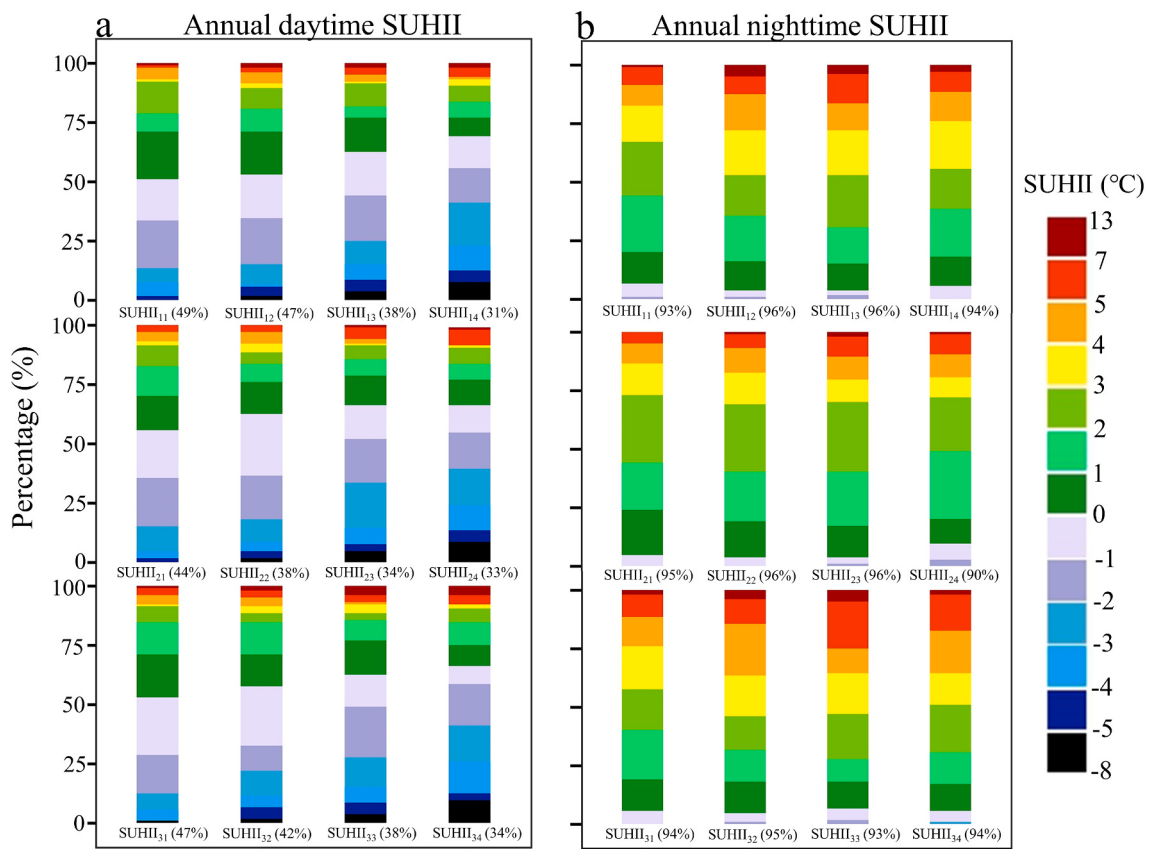


Fig. 2. Percentage-stacked bar chart of SUHII estimates based on different urban and/or rural area definitions. SUHII_{ij} denotes the estimation derived from the *i*th urban definition and the *j*th rural definition. The texts in parentheses after SUHII_{ij} note the percentages of cities exhibiting a heat island effect (i.e., SUHII >0).

when transitioning from SUHII₃₁ to SUHII₂₄ during annual daytime. These results underscored the substantial influence of urban or rural definitions on SUHII estimates for cities located in the arid zone, and a detailed analysis of the uncertainty introduced by it was provided below.

4.2. Uncertainty in SUHII estimates caused by rural definitions

By holding the urban definition constant, the average absolute difference in SUHII estimates resulting from different rural definitions was calculated, denoting this as the SUHII uncertainty induced by rural definitions, represented by ΔSUHII_R . The spatial distribution, diurnal difference, and seasonal contrast of ΔSUHII_R corresponding to different urban definitions exhibited similar patterns (Fig. 4 and Fig. 5). Notably, ΔSUHII_R surpassed 0.5 °C in the majority (50 %–84 %) of arid cities for all periods (Fig. 5a).

During the daytime, ΔSUHII_R exhibited notable spatial variations, with larger values concentrated in arid cities located in the North American and Central Asian regions (Fig. 4). Approximately half of the arid cities experienced an annual daytime ΔSUHII_R exceeding 1 °C, with a few cities surpassing even 3 °C (Fig. 5a). On a global average for arid cities, the annual daytime ΔSUHII_R reached 1.21 ± 0.17 °C (urban1), 1.19 ± 0.19 °C (urban2), and 1.25 ± 0.17 °C (urban3), respectively (Fig. 5b). Taken together, the average uncertainties induced by rural definitions in SUHII estimations during annual daytime reached 1.21 ± 0.16 °C. Besides, daytime ΔSUHII_R showed pronounced seasonal contrast, with the summer averages being approximately more than twice of those in winter (Fig. 5b).

Compared to the daytime results, the nighttime ΔSUHII_R demonstrated a smaller magnitude, accompanied by a low degree of spatial

variation, with values below 1 °C in more than three-quarters of the arid cities (Fig. 5a). On average for arid cities globally, the annual nighttime ΔSUHII_R was recorded as 0.77 ± 0.09 °C (urban1), 0.72 ± 0.11 °C (urban2), and 0.78 ± 0.10 °C (urban3), respectively (Fig. 5b). Taken together, the average uncertainties arising from rural definitions in annual nighttime SUHII estimates were 0.75 ± 0.09 °C. Moreover, unlike daytime, nighttime average ΔSUHII_R remained comparable between summer and winter (Fig. 5b).

The uncertainty in SUHII estimates induced by rural definitions may result in changes in their signs, introducing potential inconsistencies regarding identification of heat and cold islands. It was found that approximately 22 % to 32 % of all arid cities experienced a sign reversal in daytime SUHII estimates, while about 5.8 % to 10.6 % exhibited a sign reversal in nighttime SUHII estimates.

4.3. Uncertainty in SUHII estimates caused by urban definitions

By holding the rural definition constant, the average absolute difference in SUHII estimates resulting from different urban definitions was calculated, which is the SUHII uncertainty induced by urban definitions and represented by ΔSUHII_U . Unlike ΔSUHII_R , daytime and nighttime ΔSUHII_U exhibited similar magnitudes, with approximately 30–40 % of arid cities showing ΔSUHII_U exceeding 1 °C for both annual daytime and nighttime (Fig. 6 and Fig. 7). On average, annual daytime ΔSUHII_U reached 0.93 ± 0.13 °C (rural1), 0.88 ± 0.13 °C (rural2), 0.93 ± 0.14 °C (rural3), and 1.11 ± 0.19 °C (rural4), respectively (Fig. 7b). Similarly, annual nighttime ΔSUHII_U was 0.78 ± 0.13 °C (rural1), 0.90 ± 0.14 °C (rural2), 1.01 ± 0.16 °C (rural3), and 1.02 ± 0.15 °C (rural4), respectively (Fig. 7b). Taken together, the average uncertainties induced by urban definitions in SUHII estimations during annual daytime reached

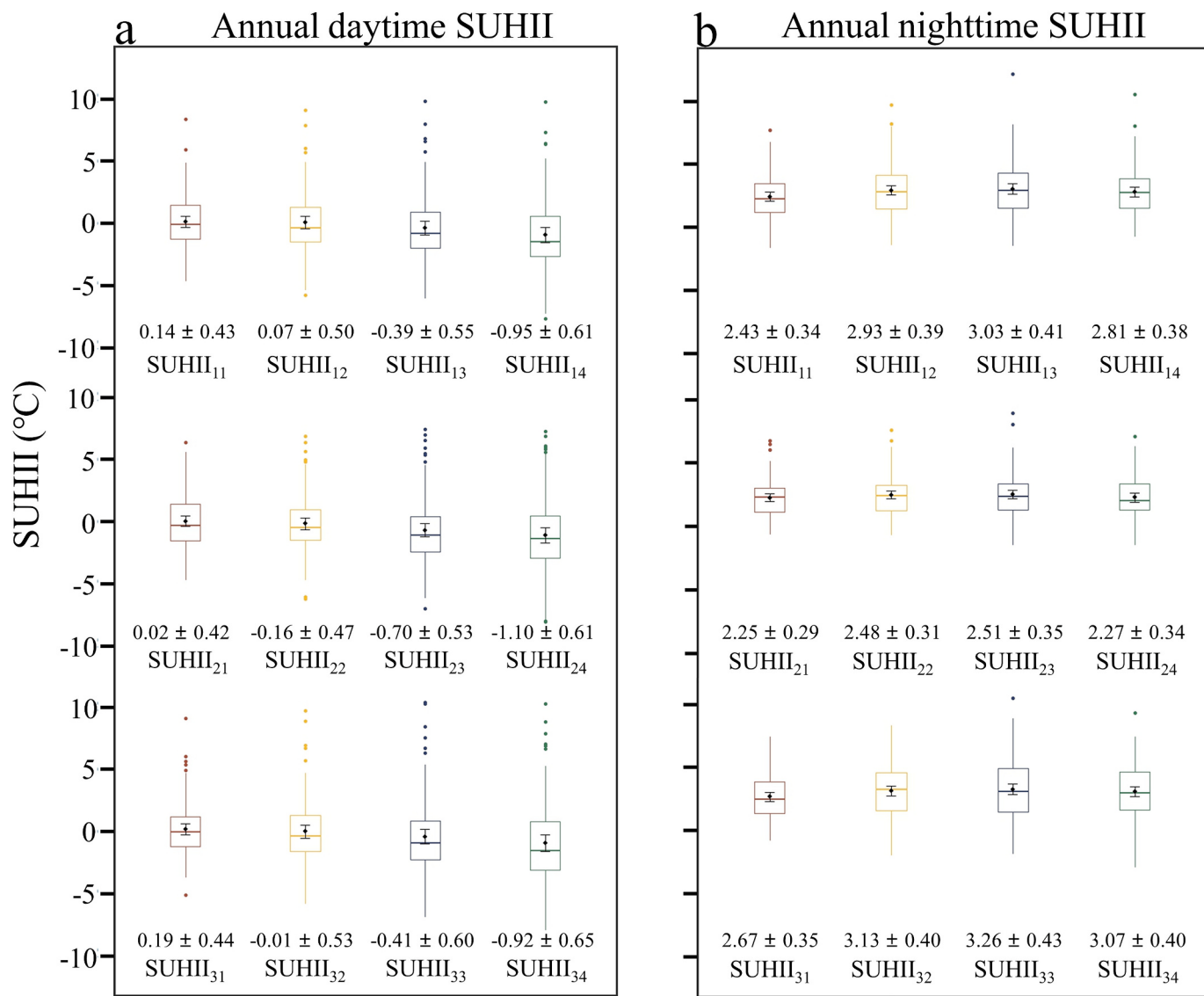


Fig. 3. Boxplot of SUHII estimates based on different urban and/or rural definitions. SUHII_{ij} denotes the estimation derived from the *i*th urban definition and the *j*th rural definition. The numerical values under the boxplot represent the mean ± 95 % confidence intervals. The central points and error bars in the boxes represent the average values and 95 % confidence intervals of the SUHII estimates, respectively.

Table 3

Seasonal averages (± 95 % confidence intervals, °C) of SUHII estimates derived by different combinations of urban and rural definitions.

Period		rural1	rural2	rural3	rural4
Summer day	urban1	-0.22 ± 0.43	-0.50 ± 0.52	-1.29 ± 0.55	-2.20 ± 0.68
	urban2	-0.42 ± 0.46	-0.81 ± 0.49	-1.72 ± 0.55	-2.42 ± 0.69
	urban3	-0.18 ± 0.41	-0.60 ± 0.53	-1.39 ± 0.61	-2.26 ± 0.68
Summer night	urban1	2.01 ± 0.20	2.27 ± 0.22	2.27 ± 0.24	2.11 ± 0.25
	urban2	1.78 ± 0.18	1.88 ± 0.17	1.84 ± 0.21	1.65 ± 0.23
	urban3	2.19 ± 0.19	2.39 ± 0.22	2.41 ± 0.24	2.24 ± 0.26
Winter day	urban1	-0.40 ± 0.27	-0.46 ± 0.31	-0.55 ± 0.36	-0.71 ± 0.39
	urban2	-0.40 ± 0.25	-0.47 ± 0.28	-0.56 ± 0.33	-0.61 ± 0.36
	urban3	-0.30 ± 0.25	-0.46 ± 0.31	-0.52 ± 0.36	-0.65 ± 0.40
Winter night	urban1	1.72 ± 0.20	2.06 ± 0.22	2.16 ± 0.25	2.15 ± 0.27
	urban2	1.55 ± 0.17	1.73 ± 0.17	1.84 ± 0.21	1.80 ± 0.22
	urban3	1.91 ± 0.20	2.22 ± 0.23	2.37 ± 0.27	2.32 ± 0.28

0.96 ± 0.13 °C and reached 0.93 ± 0.13 °C during annual nighttime. In terms of seasonal variation, summertime ΔSUHII_U was, on average, approximately twice that of wintertime during the daytime, while showing similar average values at nighttime (Fig. 7b). The uncertainties

caused by urban definitions can cause changes in the sign of SUHII estimates. It was found that about 18 % to 29 % of all arid cities experienced a sign reversal in daytime SUHII estimates, while about 1.0 % to 13.5 % exhibited a sign reversal in nighttime SUHII estimates.

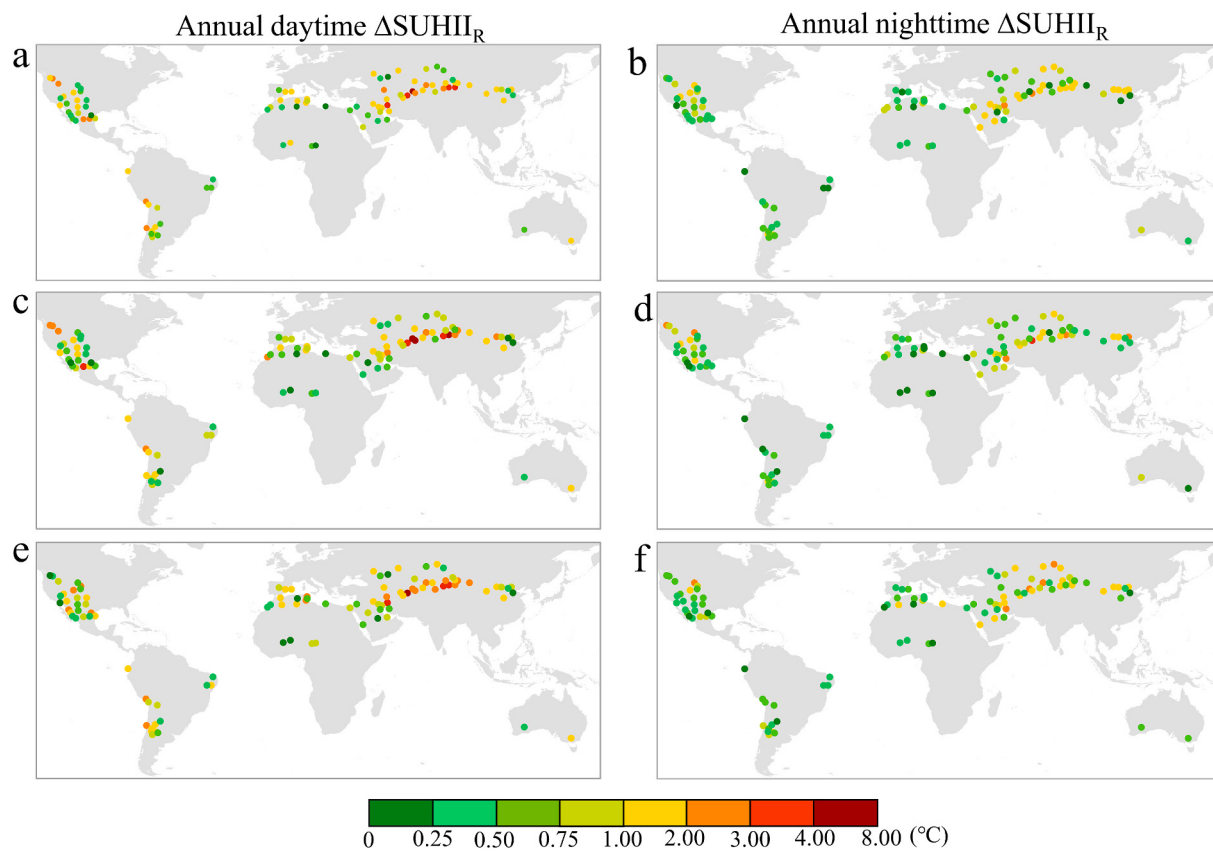


Fig. 4. Spatial distribution of ΔSUHII_R across global arid cities. ΔSUHII_R represents the average absolute difference in SUHII estimates among methods, where the rural definition varies while the urban definition keeps constant. ΔSUHII_R reflects the uncertainty caused by rural definitions. In the first row (a-b), second row (c-d), and third row (e-f), ΔSUHII_R values are presented with urban definitions fixed as urban1, urban2, and urban3, respectively.

4.4. Uncertainty in SUHII estimates caused by co-variation of urban and rural definitions

There are a total of 12 different SUHII estimates that can be derived based on different urban and rural definitions. The average absolute difference between these SUHII estimates was denoted as the uncertainty induced by co-variation of urban and rural definitions, represented as ΔSUHII_{UR} . It was observed that nearly 60 % of arid cities experienced ΔSUHII_{UR} exceeding 1 °C during annual daytime, and about 50 % during annual nighttime (Fig. 8c). On average, for arid cities globally, the uncertainties in SUHII induced by the co-variation of urban and rural definitions were 1.35 ± 0.14 °C and 1.03 ± 0.10 °C during annual daytime and nighttime (Fig. 8d), respectively, surpassing those induced by changes in the two individually.

In terms of seasonal variation, the summer daytime ΔSUHII_{UR} reached 1.84 ± 0.22 °C, which was significantly ($p < 0.001$) higher than the winter daytime ΔSUHII_{UR} . Similarly, the summer nighttime ΔSUHII_{UR} (0.80 ± 0.07 °C) was also higher than the winter nighttime ΔSUHII_{UR} (0.76 ± 0.07 °C), though their difference was not statistically significant ($p = 0.448$).

The 12 different SUHII estimates in each arid city were assessed for whether their signs of SUHII estimates changed. It was found that, under the co-variation of urban and rural definitions, the percentages of cities with sign reversals in daytime SUHII estimates were 51.0 % (annual), 51.0 % (summer), and 43.3 % (winter), respectively. Meanwhile, the percentages of cities with sign reversals in nighttime SUHII estimates were 17.3 % (annual), 17.3 % (summer), and 14.4 % (winter), respectively.

5. Discussion

5.1. Possible reasons for the high uncertainty in SUHII estimates in arid cities

The results of this study clearly demonstrated that SUHII estimates for arid cities are significantly influenced by the definitions used to select urban and rural areas. More importantly, the uncertainty caused by urban and rural definitions can lead to a change in the sign of the estimated SUHII. This can cause a reversal from heat to cold islands (and vice versa) in nearly 50 % of arid cities during the daytime and approximately 16 % of arid cities during nighttime. This high uncertainty in the estimated SUHII for arid cities is precisely because of the special land cover patterns and the small signal of the SUHI in these cities. Unlike other climatic zones, the suburbs of many arid cities are usually covered by deserts composed of bare soil and sand (a few are vegetated) due to the lack of water (Li, 2003; Liu et al., 2021; Jones et al., 2023). When the sun shines directly on the earth's surface during the day, the sand with a small specific heat capacity will quickly absorb heat and increase the LST, making it higher than that in urban areas, and so as to form an urban cold island. At night, the heat in the desert will dissipate rapidly, causing the temperature to drop sharply, which will be lower than the urban LST, so as to form an urban heat island (Zandi et al., 2023). This phenomenon can also be clearly seen from the day and night comparison results in Table 3 of this study. Complex land cover composition may lead to significant spatial heterogeneity in surface temperatures around urban areas in arid zones. As a result, changes in the extent of urban and rural areas can lead to dramatic fluctuations in LST within them that in turn can cause changes in the magnitude and even the sign of the estimated SUHII.

To gain further insight into the causes of the high uncertainty in UHII

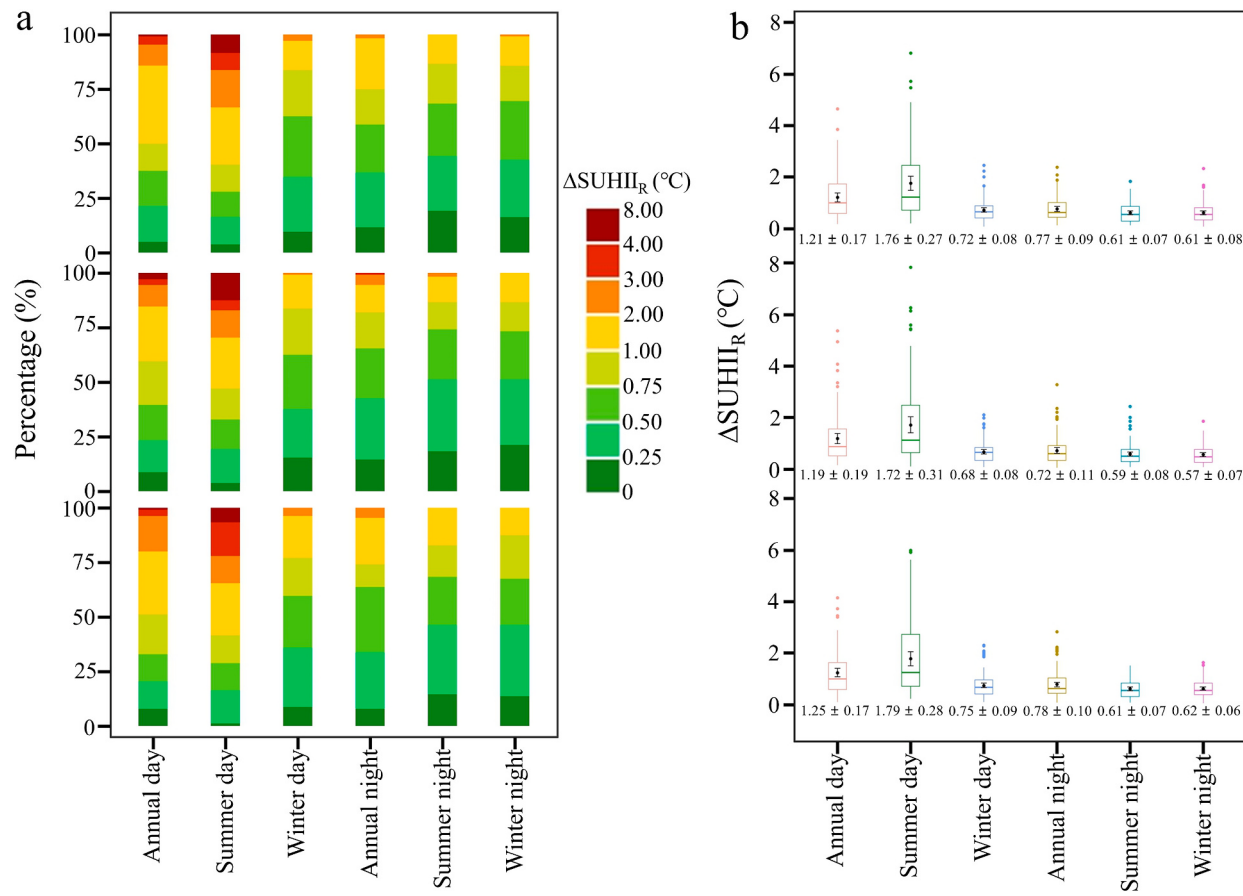


Fig. 5. Diurnal and seasonal contrasts of ΔSUHII_R across global arid cities. ΔSUHII_R represents the average absolute difference in SUHII estimates among methods, where the rural definition varies while the urban definition keeps constant. ΔSUHII_R reflects the uncertainty caused by rural definitions. In each subplot, the first, second, and third rows display ΔSUHII_R values with urban definitions fixed as urban1, urban2, and urban3, respectively. The numerical values in (b) represent the mean \pm 95 % confidence intervals. The central points and error bars in the boxes represent the average values and 95 % confidence intervals of the ΔSUHII_R , respectively.

in arid cities, we included two surface properties, EVI and WSA, which have been reported to be important factors influencing LST (Peng et al., 2012; Yang and Zhao, 2023; Yang et al., 2019; Yao et al., 2019; Zhou et al., 2014). Similar to SUHII, we calculated the urban-rural differences in EVI (referred to as DiffEVI) and WSA (referred to as DiffWSA) for each city. In addition, similar to $\Delta\text{SUHII}_{U,R}$, we computed the mean absolute differences for each city between DiffEVI and between DiffWSA obtained under the 12 different urban and rural definitions, noting them as $\Delta\text{DiffEVI}_{U,R}$ and $\Delta\text{DiffWSA}_{U,R}$, respectively. These two metrics reflect the uncertainty in DiffEVI and DiffWSA induced by co-variation of urban and rural definitions, respectively. As depicted in Fig. 9, both DiffEVI and DiffWSA demonstrated significant variations under different urban and rural definitions, which aligned with the overall trend of SUHII. Specifically, as depicted in Fig. 3, the mean values of annual daytime and nighttime SUHII generally exhibited a decreasing and increasing trend, respectively, as the definition of rural area shifted from rural1 to rural3. Concurrently, as illustrated in Fig. 9, the mean values of DiffEVI typically increased, while the mean values of DiffWSA typically decreased, as the rural definition changed from rural1 to rural3. Fig. 10 shows the spatial patterns of $\Delta\text{DiffEVI}_{U,R}$ and $\Delta\text{DiffWSA}_{U,R}$. It is evident that both $\Delta\text{DiffEVI}_{U,R}$ and $\Delta\text{DiffWSA}_{U,R}$ exhibited high values in arid cities across the North America and Central Asia, with a spatial distribution similar to that of $\Delta\text{SUHII}_{U,R}$ (Fig. 8). Further spearman correlation analysis revealed a significant ($p < 0.05$) positive relationship between $\Delta\text{SUHII}_{U,R}$ and $\Delta\text{DiffEVI}_{U,R}$ or $\Delta\text{DiffWSA}_{U,R}$ (Fig. 10). Specifically, $\Delta\text{DiffEVI}_{U,R}$ exhibited a higher correlation coefficient with $\Delta\text{SUHII}_{U,R}$ compared to $\Delta\text{DiffWSA}_{U,R}$, emphasizing the important role of

the vegetation index on heat islands (Fig. 10). For seasonal comparisons, the correlation between $\Delta\text{SUHII}_{U,R}$ and $\Delta\text{DiffEVI}_{U,R}$ was much stronger in summer than in winter (Figs. S2–3), consistent with the seasonal patterns in vegetation activity. In contrast, the correlation between $\Delta\text{SUHII}_{U,R}$ and $\Delta\text{DiffWSA}_{U,R}$ remained relatively consistent across seasons, showing a weak positive relationship (Figs. S2–3).

Taken together, the analysis suggests that variations in urban and rural definitions can influence their respective land covers, thereby impacting surface properties such as EVI and WSA. These variations can lead to differences in average LST within urban and rural areas, consequently contributing to uncertainties in the estimated SUHII. To illustrate these ideas more intuitively, we used two arid cities as examples to explore variations in land cover, surface properties, and SUHII estimates under different urban and rural definitions. In Fig. 11, a representative city demonstrated a notable variation in the spatial extent of its rural areas under different rural definitions. These variations led to changes in both the distribution and composition of land covers within different rural areas. Specifically, with the transition from rural1 to rural4, there was a gradual decline in the proportion of vegetation within the rural area, accompanied by a corresponding increase in the proportion of bare lands (Fig. 11c). This change in land cover composition led to a decrease in rural EVI and an increase in rural WSA, resulting in a larger DiffEVI and a smaller DiffWSA (Fig. 11b). SUHII was typically negatively correlated with DiffEVI and positively correlated with DiffWSA (Peng et al., 2012; Zhou et al., 2014). Consequently, SUHII showed an obvious increasing trend when transforming from rural1 to rural4, with its highest value of 2.50 °C based on rural1 and its lowest value of –6.13 °C

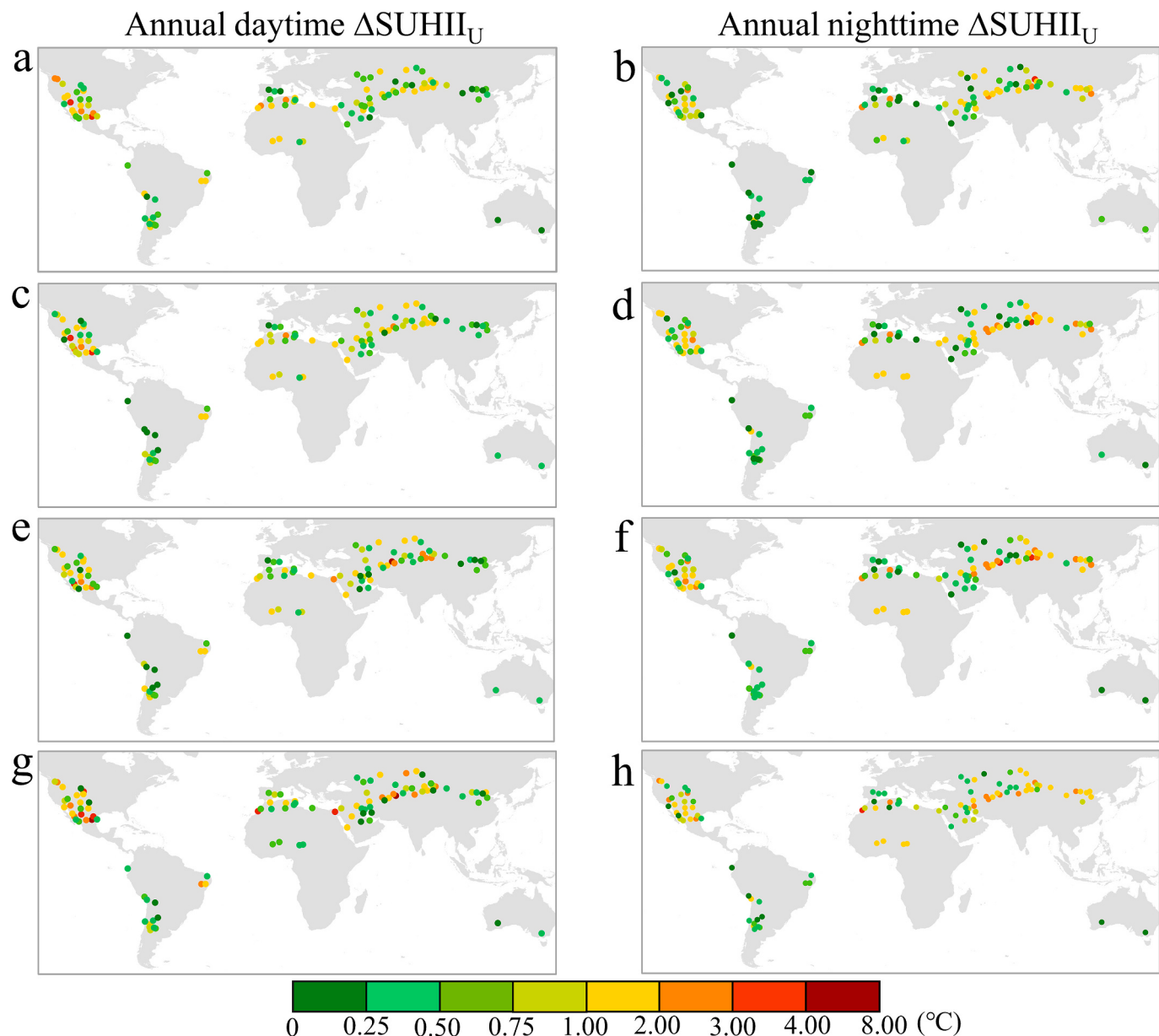


Fig. 6. Spatial distributions of ΔSUHII_U across global arid cities. ΔSUHII_U represents the average absolute difference in SUHII estimates among methods, where the urban definition varies while the rural definition keeps constant. ΔSUHII_U reflects the uncertainty caused by rural definitions. In the first row (a-b), second row (c-d), third row (e-f), and fourth row (g-h), ΔSUHII_U values are presented with rural definitions fixed as rural1, rural2, rural3, and rural4, respectively.

based on rural4 (Fig. 11b). Fig. 12 illustrates an example of how urban definitions influence SUHII estimates. Despite the prevalence of artificial surfaces within the boundaries of all urban areas, modifying their definitions can still lead to changes in the distribution of other land covers within these areas (Fig. 12c). The modification of land cover proportions can lead to a change in the DiffEVI and DiffWSA inside the urban area, which further caused a change in the estimated SUHII (Fig. 12b). However, the alterations in land cover resulted from urban definitions were relatively weaker than that caused by rural definitions, which partially elucidated why the uncertainty stemming from rural definitions is generally higher than that arising from urban definitions.

To summarize, modifications in urban and rural definitions directly impact their land cover and surface properties, resulting in shifts in their average LSTs that, in turn, contribute to variations in the estimated SUHII. The complexity of land cover types in/around arid cities can amplify such variations in LST, consequently contributing to elevated uncertainties in SUHII estimates. Additionally, the topography of

mountainous cities is characterized by substantial undulations, resulting in considerable variations in the elevations of rural areas based on different definitions. Even though areas with elevation anomalies have been excluded during the rural selection process, the notable topographic relief in mountainous cities may still exert influences on the estimation of SUHII (Yang et al., 2023b).

5.2. Implications and contributions

Firstly, this study provides a global-scale survey on the SUHI effect in arid cities based on multiple remote sensing products and diversified urban-rural definition methods. Previous studies have predominantly focused on the separate effects of rural or urban definitions on SUHII estimates (Schwarz et al., 2011; Yao et al., 2018; Li et al., 2019; Li et al., 2022; Yang et al., 2023b; Liu et al., 2023; Yang et al., 2023a). This study, however, is the first to analyze the combined effects of urban and rural definitions on the estimated SUHII. Our findings revealed that the

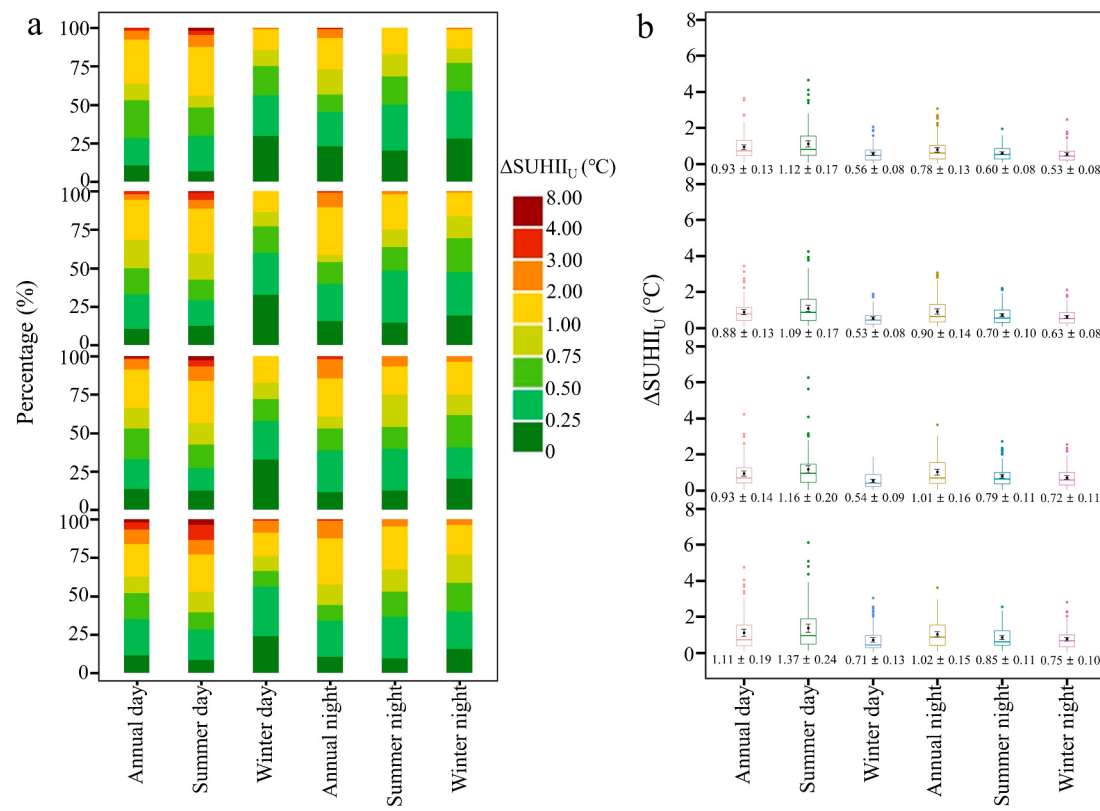


Fig. 7. Diurnal and seasonal contrasts of ΔSUHII_U across global arid cities. ΔSUHII_U represents the average absolute difference in SUHII estimates among methods, where the urban definition varies while the rural definition keeps constant. ΔSUHII_U reflects the uncertainty caused by urban definitions. In each subplot, the first, second, third, and fourth rows display ΔSUHII_U values with rural definitions fixed as rural1, rural2, rural3, and urban4, respectively. The numerical values in (b) represent the mean \pm 95 % confidence intervals. The central points and error bars in the boxes represent the average values and 95 % confidence intervals of the ΔSUHII_U , respectively.

uncertainty arising from simultaneous variations in both urban and rural definitions was generally higher than that resulting from their individual changes. These results contribute to a more comprehensive understanding of the quantitative approach to SUHII quantification.

Secondly, this study offers new insights into the ongoing debate on heat and cold islands in arid cities. Previous studies focused on arid cities have not reached consensus on the spatial patterns and magnitudes of the estimated SUHII, and even provided contradictory observations between cold and heat islands (Sofer and Potchter, 2006; Rasul et al., 2017; Chen et al., 2023; Reisi et al., 2019). By analyzing over a hundred global arid cities, this study showed that the identification of UHI or UCI depended largely on the choice of urban and rural definitions. This provides a plausible explanation for the inconsistency between previous analyses of the SUHII estimates in arid cities.

Thirdly, this study emphasizes the importance of constructing a unified and scientific urban-rural division method for heat island research. The heat island signal of arid cities is low, thus the determination of their UHI or UCI effect is more sensitive to the definition of the urban-rural boundary than cities in other climate zones. Therefore, we suggest that maintaining the “purity” of the selected urban and rural areas is crucial for reducing uncertainty in the estimated SUHII for arid cities. One potential approach is to define urban and rural areas based on the local climate zone (LCZ) classification system, which categorizes cities into different types (e.g., compact high-rise, heavy industry, low vegetation, etc.) based on surface coverages and structural characteristics (Bechtel et al., 2019). By defining urban or rural areas as specific LCZ subtypes rather than a mixture of types, variations in SUHII due to changes in boundaries of urban and/or rural extents can be minimized. Although this study does not provide a definitive answer on how to choose the optimal urban and rural areas, it offers possible ideas for

addressing the issue.

5.3. Limitations and future studies

First, we employed the most popular LST data, MYD11A1, for calculating the SUHII. Given the high spatiotemporal variability in LST, the results obtained by the MYD11A1 LST data may differ from those derived other LST products (Yang et al., 2024; Yao et al., 2020). The bias resulting from data discrepancies requires further analysis in future studies.

Second, this study incorporated several commonly used definitions of urban and rural areas, thereby encompassing a diverse range of SUHII estimation methods employed in existing studies. However, it should be noted that our analysis results can be influenced by the included methods. For instance, a less comprehensive inclusion of methods may introduce a bias, leading to an underestimation of the SUHII uncertainty caused by urban and rural definitions (Fig. S4). As the SUHII research progresses, new methods for quantifying this phenomenon continue to emerge (Yao et al., 2023; Yang et al., 2023b; Li et al., 2022). Future studies should integrate more methods to provide a better comprehensive analysis of SUHII uncertainty resulting from estimation methods.

Third, this study empirically required that all cities included must have an urban area $>20 \text{ km}^2$. This threshold ensures the selection of a sufficient number (more than one hundred) of major arid cities globally, but it leads to the omission of many small cities. As shown in Fig. 13, the uncertainty in SUHII caused by urban and rural definitions did not exhibit an obvious trend with increasing urban area during the daytime, but it decreased greatly with increasing urban area (from 20 km^2 to 300 km^2) during the nighttime. Thus, ignoring small cities does not appear to have a significant impact on the daytime SUHII uncertainty quantified in

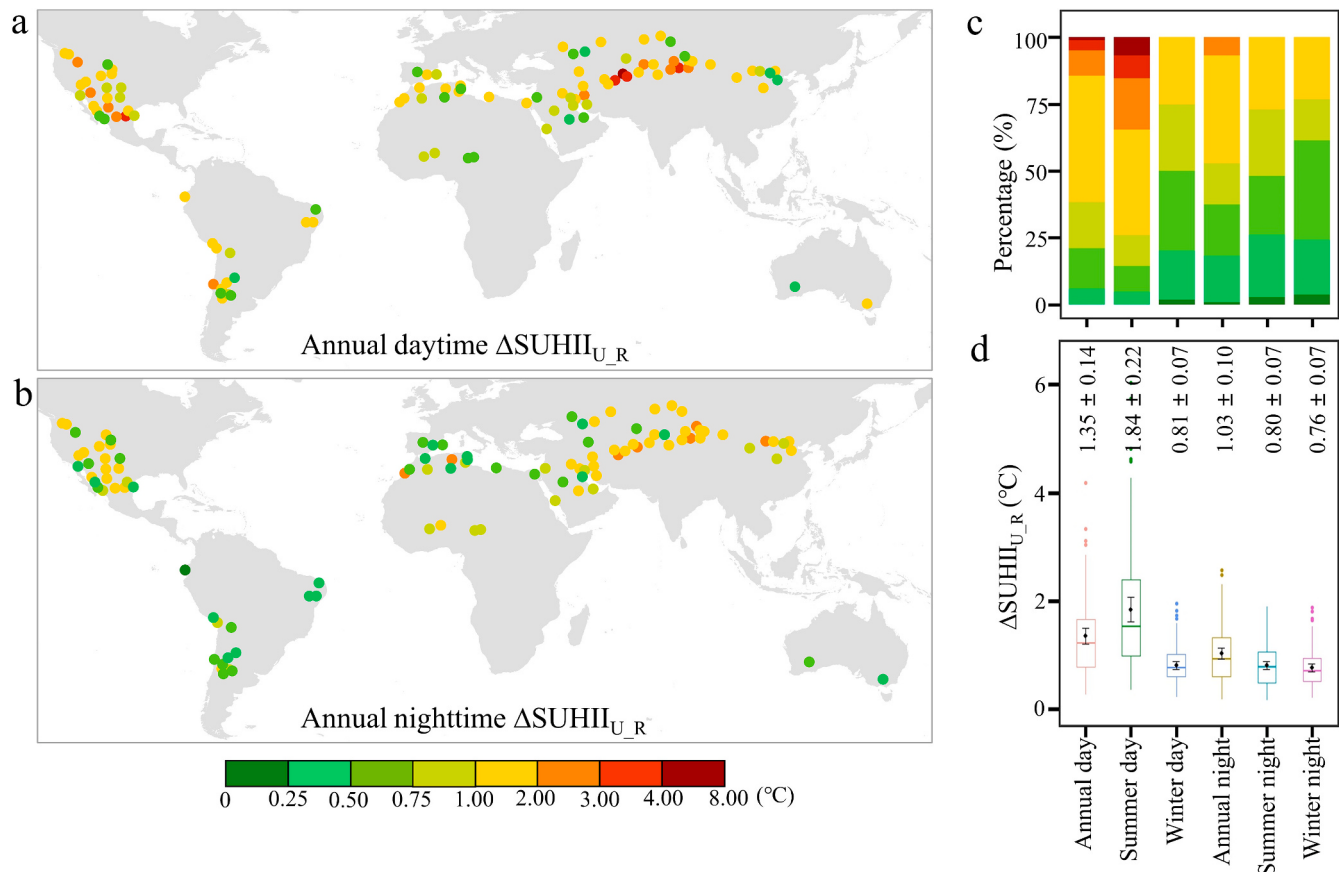


Fig. 8. Spatiotemporal patterns of ΔSUHII_{U_R} across global arid cities. (a-b) Spatial distributions of annual daytime and nighttime ΔSUHII_{U_R} . (c) Percentage-stacked bar chart of ΔSUHII_{U_R} . (d) Boxplot of ΔSUHII_{U_R} . ΔSUHII_{U_R} represents the average absolute difference in SUHII estimates among methods with different urban and rural definitions. ΔSUHII_{U_R} reflects the uncertainty caused by the co-variation of urban and rural definitions. The central points and error bars in the boxes represent the average values and 95 % confidence intervals of the ΔSUHII_{U_R} , respectively.

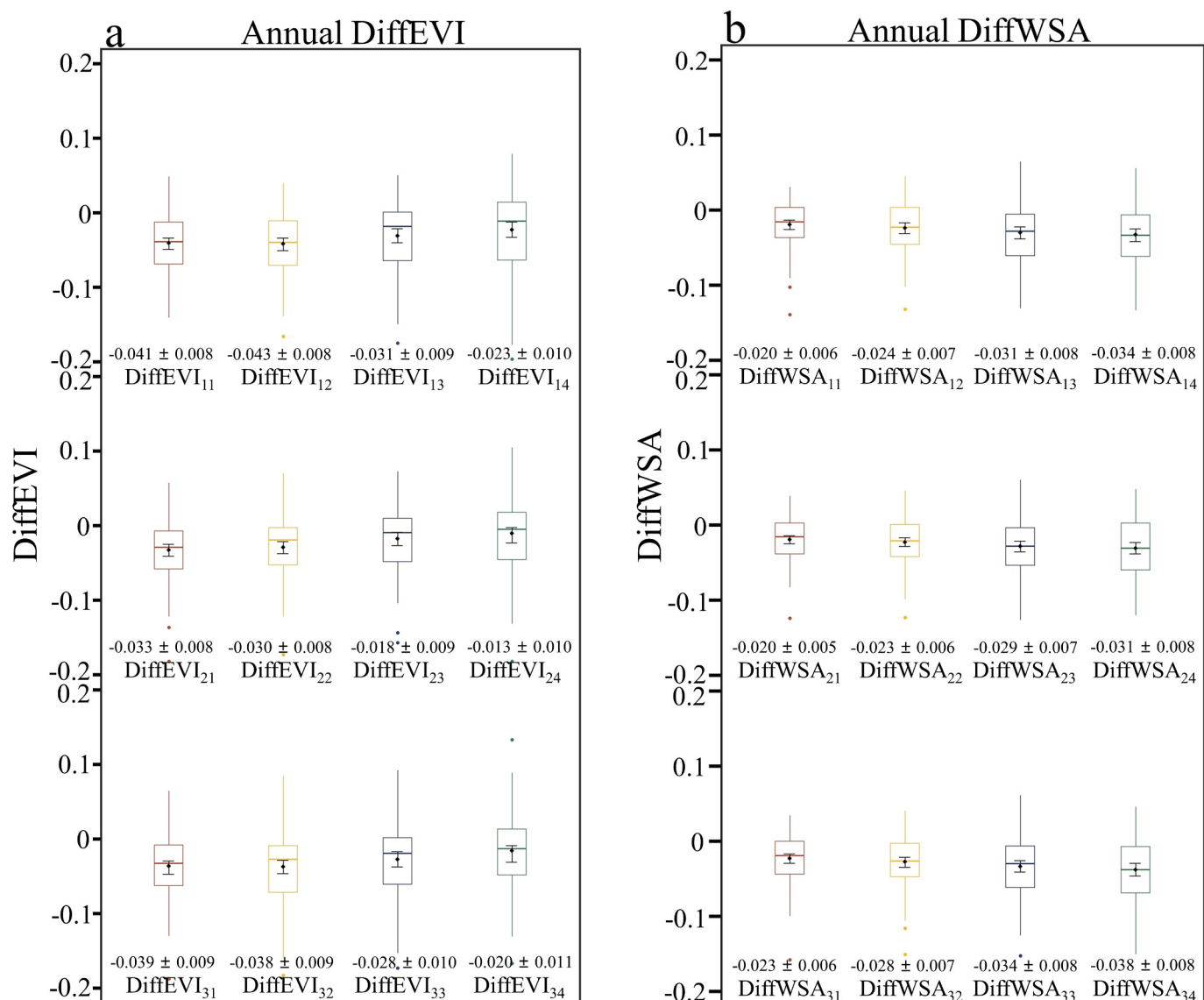


Fig. 9. Boxplots of DiffEVI and DiffWSA based on different urban and/or rural definitions. DiffEVI_{ij} or DiffWSA_{ij} denotes the urban-rural difference in EVI or WSA derived from the i th urban definition and the j th rural definition. The numerical values under the boxplots represent the mean \pm 95 % confidence intervals. The central points in the boxes refer to the mean values of the DiffEVI_{ij} or DiffWSA_{ij} for all arid cities, and the error bars denote corresponding 95 % confidence intervals.

this study, but it could potentially lead to an underestimation of the nighttime SUHII uncertainty. Furthermore, it is crucial to acknowledge that by excluding areas within rural buffers affected by disturbing factors (details in Methods), there is a notable decrease in available rural areas for some cities (see supplementary materials). The reduction in accessible rural pixels may compromise the representativeness of background climate data and potentially increase uncertainty in SUHII estimates. Hence, future research should prioritize developing a dynamic method for rural area extraction that maximizes the retention of background reference pixels while minimizing the influence of confounding factors.

Finally, this study offers a plausible explanation for the SUHII uncertainties induced by urban and rural definitions, viewed through the lens of land cover compositions and surface properties including EVI and WSA. Alterations in urban and rural extents also influence other attributes, such as human activities, regional climates, and other biophysical attributes (Li et al., 2019; Liu et al., 2018). These factors are closely linked to surface temperatures in urban and rural areas, influencing SUHII estimates (Peng et al., 2012; Zhou et al., 2014). Future analyses can be even more thorough and comprehensive by incorporating

additional datasets.

6. Conclusions

The ecological susceptibility of arid zones has prompted concerns about climate impacts of urbanization in these regions. However, existing studies on arid cities lack consensus regarding both the magnitude and sign of the SUHII estimates. This disparity has ignited an ongoing debate surrounding the question of whether urbanization in arid cities results in a local temperature increase or decrease. Therefore, we selected 104 arid cities globally to conduct a comprehensive assessment of the impact of estimation methods on the quantification of SUHII.

The findings indicated that urban and rural definitions can have a substantial impact on the estimated SUHII, resulting in an uncertainty (ΔSUHII) exceeding 1 °C in more than half of the cities. On average for global arid cities, the annual daytime and nighttime ΔSUHII induced by co-variation of urban and rural definitions reached 1.35 °C and 1.03 °C, respectively. Moreover, the uncertainty arising from urban and rural definitions can result in a reversal of the sign of estimated SUHII,

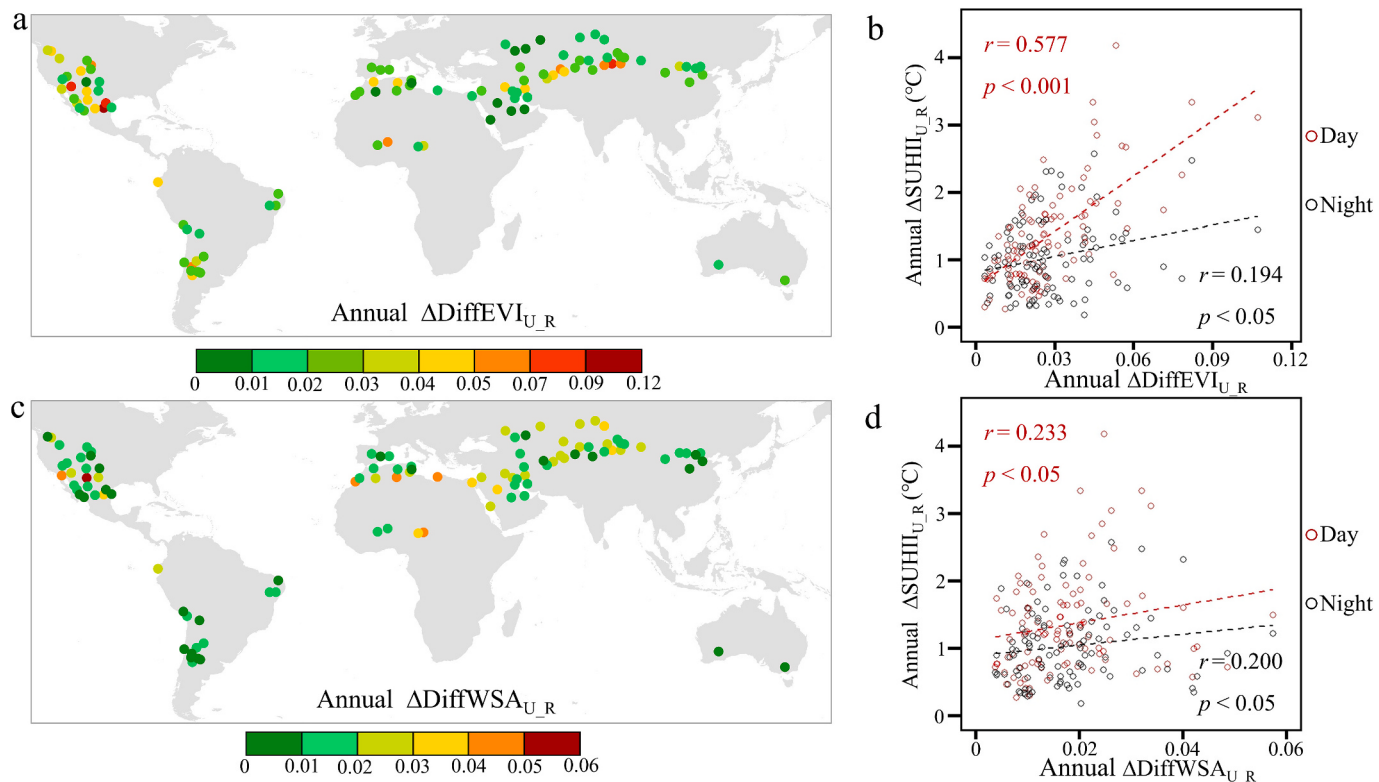


Fig. 10. Spatiotemporal patterns of $\Delta\text{DiffEVI}_{U_R}$ and $\Delta\text{DiffWSA}_{U_R}$ across global arid cities and their relation with ΔSUHII_{U_R} . (a and c) Spatial distributions of annual $\Delta\text{DiffEVI}_{U_R}$ and $\Delta\text{DiffWSA}_{U_R}$. (b) Scatterplot of ΔSUHII_{U_R} and $\Delta\text{DiffEVI}_{U_R}$ for global arid cities. (d) Scatterplot of ΔSUHII_{U_R} and $\Delta\text{DiffWSA}_{U_R}$ for global arid cities. The r represents the spearman correlation coefficient and the p represents the level of significance. ΔSUHII_{U_R} refers to the SUHII uncertainty caused by co-variation of urban and rural definitions. $\Delta\text{DiffEVI}_{U_R}$ or $\Delta\text{DiffWSA}_{U_R}$ represents the uncertainty in urban-rural difference in EVI or WSA caused by the co-variation of urban and rural definitions.

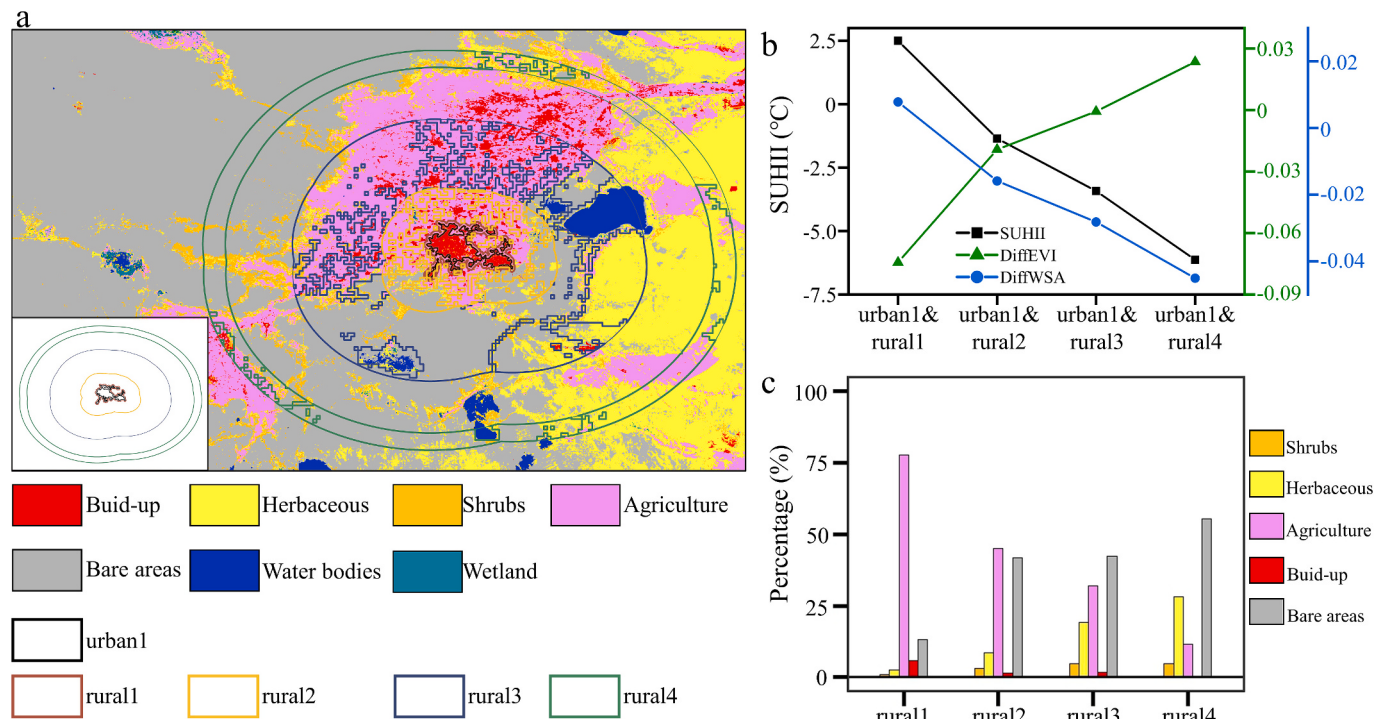


Fig. 11. The influence of rural definition on SUHII estimates, taking Bukhara, Uzbekistan as an example. (a) Spatial patterns of land covers and extents of urban and rural areas. (b) Variations of DiffEVI, DiffWSA, and SUHII estimates with different rural definitions. (c) Variations of land cover compositions with different rural definitions. DiffEVI and DiffWSA denotes the urban-rural difference in EVI and WSA, respectively.

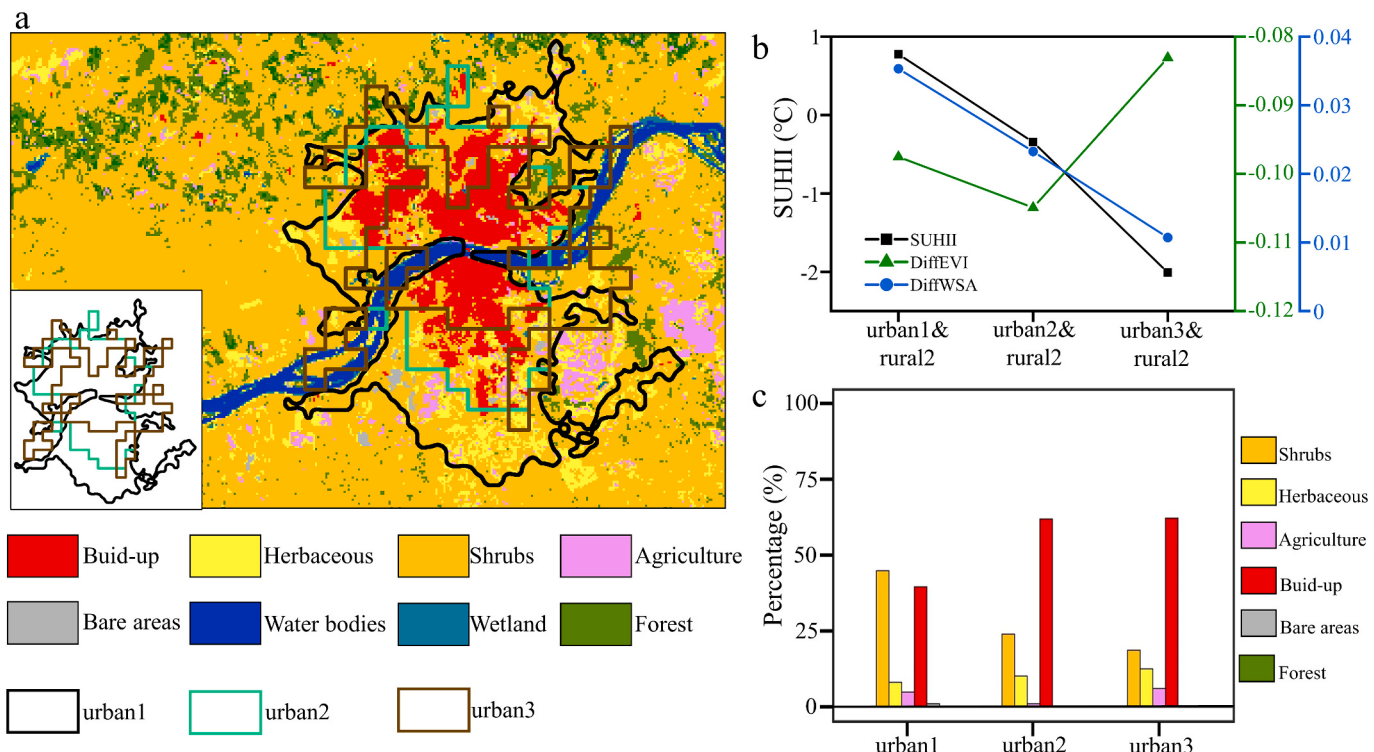


Fig. 12. The influence of urban definition on SUHII estimates, taking Petrolina-Juazeiro, Brazil as an example. (a) Spatial patterns of land covers and urban extents. (b) Variations of DiffEVI, DiffWSA, and SUHII estimates with different urban definitions. (c) Variations of land cover compositions with different urban definitions. DiffEVI and DiffWSA denotes the urban-rural difference in EVI and WSA, respectively.

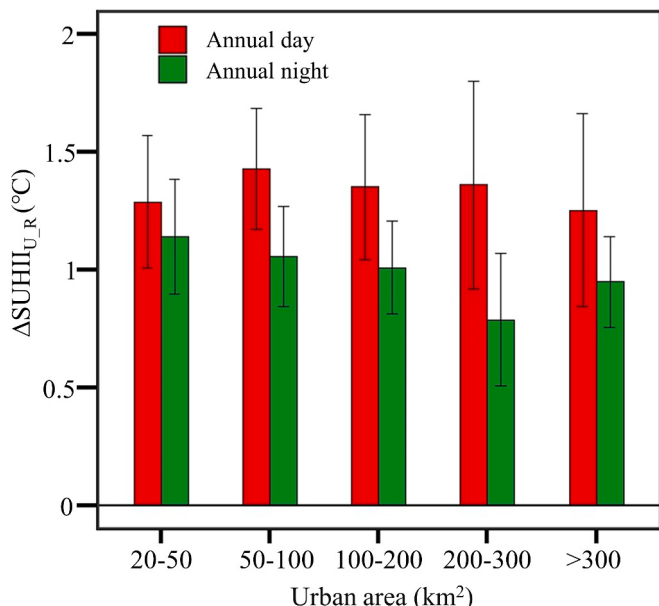


Fig. 13. Variation of $\Delta\text{SUHII}_{U,R}$ with urban area size. $\Delta\text{SUHII}_{U,R}$ refers to the SUHII uncertainty caused by co-variation of urban and rural definitions. The error bars denote corresponding 95 % confidence intervals.

indicative of a reciprocal transition between heat and cold islands. It was observed that, under different definitions of urban and rural areas, nearly 50 % of arid cities experienced a sign reversal in daytime SUHII, and about 15 % exhibited a sign reversal in nighttime SUHII. Additional analyses highlighted those variations in land covers and surface properties (vegetation index and albedo), stemming from differences in urban and rural definitions, played a crucial role in elucidating the

uncertainty in SUHII estimations. In summary, our results offered insights into the ongoing debate about urban heat and cold islands in arid zones in existing studies and underscored the importance of standardizing SUHII estimation methods.

CRediT authorship contribution statement

Zehong Liu: Writing – original draft, Software, Methodology, Investigation. **Richen Ye:** Writing – review & editing, Visualization, Resources. **Qiquan Yang:** Writing – review & editing, Writing – original draft, Methodology, Funding acquisition, Conceptualization. **Ting Hu:** Writing – review & editing, Software. **Yue Liu:** Writing – review & editing, Resources, Investigation. **TC Chakraborty:** Writing – review & editing, Formal analysis. **Zhenxuan Liao:** Writing – review & editing.

Declaration of competing interest

The authors declare that they have no known competing financial interests or personal relationships that could have appeared to influence the work reported in this paper.

Data availability

The Global Urban Boundary dataset can be downloaded from <http://data.starcloudpcl.ac.cn/zh/resource/14>. The Global Human Settlement Layer is available at <https://ghsl.jrc.ec.europa.eu/download.php?ds=ucdb>. The MODIS land cover data is available from <https://lpdaac.usgs.gov/products/mcd12q1v061/>. The MODIS LST products can be accessed from <https://e4ftl01.cr.usgs.gov/MOLA/MYD11A1.061/>. The global 30 arc-second elevation data can be downloaded from <https://www.usgs.gov/centers/eros/science/usgs-eros-archive-digital-elevation-global-30-arc-second-elevation-gtopo30>. The global surface water data can be accessed from <https://global-surface-water.appspot.com/download>. The global

impervious surface area data is available from <http://irsip.whu.edu.cn/resources/dataweb.php>. The land cover data is available from <https://lcviewer.vito.be/2018>. The Köppen-Geiger climate classification map is available from <https://www.globo2.org/koppen/>. The enhanced vegetation index (EVI) data is available from <https://doi.org/10.5067/MODIS/MYD13A2.061>. The white sky albedo (WSA) data is available from <https://doi.org/10.5067/MODIS/MCD43A3.061>. All the other data can be accessed from the Google Earth Engine platform (<https://code.earthengine.google.com/>). All data are available upon reasonable request from the authors.

Acknowledgments

This research was supported by the Postdoctoral Science Foundation of China (2023M730735, 2021TQ0245, and 2021M702470), and the Key-Area Research and Development Program of Guangdong Province (2020B0101130009). T.C.'s contribution was supported by the U.S. Department of Energy (DOE), Office of Science, Biological and Environmental Research program through the Early Career Research Program. Pacific Northwest National Laboratory is operated for DOE by Battelle Memorial Institute under contract DE-AC05-76RL01830.

Appendix A. Supplementary data

Supplementary data to this article can be found online at <https://doi.org/10.1016/j.scitotenv.2024.175631>.

References

- Abulibdeh, A., 2021. Analysis of urban heat island characteristics and mitigation strategies for eight arid and semi-arid gulf region cities. *Environ. Earth Sci.* 80, 1–26.
- Bakarman, M.A., Chang, J.D., 2015. The influence of height/width ratio on urban heat island in hot-arid climates. *Procedia Eng.* 118, 101–108.
- Bechtel, B., Demuzere, M., Mills, G., Zhan, W., Sismanidis, P., Small, C., Voogt, J., 2019. SUHI analysis using local climate zones—a comparison of 50 cities. *Urban Clim.* 28, 100451.
- Beck, H.E., Zimmermann, N.E., McVicar, T.R., Vergopolan, N., Berg, A., Wood, E.F., 2018. Present and future Köppen-Geiger climate classification maps at 1-km resolution. *Sci. Data* 5 (1), 1–12.
- Buchhorn, M., Lesiv, M., Tsendbazar, N.-E., Herold, M., Bertels, L., Smets, B., 2020. Copernicus global land cover layers—collection 2. *Remote Sens.* 12, 1044.
- Campos, J.C., Brito, J.C., 2018. Mapping underrepresented land cover heterogeneity in arid regions: the Sahara-Sahel example. *ISPRS J. Photogramm. Remote Sens.* 146, 211–220.
- Chakraborty, T., Hsu, A., Manya, D., Sheriff, G., 2020. A spatially explicit surface urban heat island database for the United States: characterization, uncertainties, and possible applications. *ISPRS J. Photogramm. Remote Sens.* 168, 74–88.
- Chakraborty, T., Lee, X., 2019. A simplified urban-extent algorithm to characterize surface urban heat islands on a global scale and examine vegetation control on their spatiotemporal variability. *Int. J. Appl. Earth Obs. Geoinf.* 74, 269–280.
- Chakraborty, T., Sarangi, C., Lee, X., 2021. Reduction in human activity can enhance the urban heat island: insights from the COVID-19 lockdown. *Environ. Res. Lett.* 16, 054060.
- Chen, X.-L., Zhao, H.-M., Li, P.-X., Yin, Z.-Y., 2006. Remote sensing image-based analysis of the relationship between urban heat island and land use/cover changes. *Remote Sens. Environ.* 104, 133–146.
- Chen, Y., Xie, M., Chen, B., Wang, H., Teng, Y., 2023. Surface regional heat (cool) island effect and its diurnal differences in arid and semiarid resource-based urban agglomerations. *Chin. Geogr. Sci.* 33, 131–143.
- Clinton, N., Gong, P., 2013. MODIS detected surface urban heat islands and sinks: global locations and controls. *Remote Sens. Environ.* 134, 294–304.
- Dialesandro, J.M., Wheeler, S.M., Abunnasr, Y., 2019. Urban heat island behaviors in dryland regions. *Environ. Res. Commun.* 1, 081005.
- Dihkan, M., Karsli, F., Guneroglu, A., Guneroglu, N., 2015. Evaluation of surface urban heat island (SUHI) effect on coastal zone: the case of Istanbul megacity. *Ocean Coast. Manag.* 118, 309–316.
- Du, H., Zhan, W., Liu, Z., Li, J., Li, L., Lai, J., Miao, S., Huang, F., Wang, C., Wang, C., 2021. Simultaneous investigation of surface and canopy urban heat islands over global cities. *ISPRS J. Photogramm. Remote Sens.* 181, 67–83.
- Duan, S.-B., Li, Z.-L., Wu, H., Leng, P., Gao, M., Wang, C., 2018. Radiance-based validation of land surface temperature products derived from collection 6 MODIS thermal infrared data. *Int. J. Appl. Earth Obs. Geoinf.* 70, 84–92.
- Florczyk, A., Melchiorri, M., Corbane, C., Schiavina, M., Maffenini, M., Pesaresi, M., Politis, P., Sabo, S., Freire, S., Ehrlich, D., 2019. Description of the GHS urban Centre database 2015. Public Release 1, 1–75.
- Gaur, M.K., Squires, V.R., 2018. Geographic extent and characteristics of the world's arid zones and their peoples. *Climate Variability Impacts on Land use and Livelihoods in Drylands* 3–20.
- Geng, X., Zhang, D., Li, C., Yuan, Y., Yu, Z., Wang, X., 2023. Impacts of climatic zones on urban heat island: spatiotemporal variations, trends, and drivers in China from 2001–2020. *Sustain. Cities Soc.* 89, 104303.
- Gong, P., Li, X., Wang, J., Bai, Y., Chen, B., Hu, T., Liu, X., Xu, B., Yang, J., Zhang, W., 2020. Annual maps of global artificial impervious area (GAIA) between 1985 and 2018. *Remote Sens. Environ.* 236, 111510.
- Hu, J., Yang, Y., Zhou, Y., Zhang, T., Ma, Z., Meng, X., 2022. Spatial patterns and temporal variations of footprint and intensity of surface urban heat island in 141 China cities. *Sustain. Cities Soc.* 77, 103585.
- Huang, X., Song, Y., Yang, J., Wang, W., Ren, H., Dong, M., Feng, Y., Yin, H., Li, J., 2022. Toward accurate mapping of 30-m time-series global impervious surface area (GISA). *Int. J. Appl. Earth Obs. Geoinf.* 109, 102787.
- Imhoff, M.L., Zhang, P., Wolfe, R.E., Bounoua, L., 2010. Remote sensing of the urban heat island effect across biomes in the continental USA. *Remote Sens. Environ.* 114, 504–513.
- Jin, M., Dickinson, R.E., Zhang, D., 2005. The footprint of urban areas on global climate as characterized by MODIS. *J. Clim.* 18, 1551–1565.
- Jones, D.L., Fuentes, B., Arenas-Díaz, F., Remondel, F., van Hall, R., Atkinson, B.S., Mooney, S.J., Bol, R., 2023. Life at the extreme: plant-driven hotspots of soil nutrient cycling in the hyper-arid core of the Atacama Desert. *Soil Biol. Biochem.* 184, 109128.
- Kottek, M., Grieser, J., Beck, C., Rudolf, B., Rubel, F., 2006. World map of the Köppen-Geiger climate classification updated. *Meteorol. Z.* 15 (3), 259–263.
- Lai, J., Zhan, W., Huang, F., Voogt, J., Bechtel, B., Allen, M., Peng, S., Hong, F., Liu, Y., Du, P., 2018. Identification of typical diurnal patterns for clear-sky climatology of surface urban heat islands. *Remote Sens. Environ.* 217, 203–220.
- Lai, J., Zhan, W., Voogt, J., Quan, J., Huang, F., Zhou, J., Bechtel, B., Hu, L., Wang, K., Cao, C., 2021. Meteorological controls on daily variations of nighttime surface urban heat islands. *Remote Sens. Environ.* 253, 112198.
- Lazzarini, M., Molini, A., Marpu, P.R., Ouarda, T.B., Ghedira, H., 2015. Urban climate modifications in hot desert cities: the role of land cover, local climate, and seasonality. *Geophys. Res. Lett.* 42, 9980–9989.
- Li, K., Chen, Y., 2023. Identifying and characterizing frequency and maximum durations of surface urban heat and cool island across global cities. *Sci. Total Environ.* 859, 160218.
- Li, K., Chen, Y., Gao, S., 2022. Uncertainty of city-based urban heat island intensity across 1112 global cities: background reference and cloud coverage. *Remote Sens. Environ.* 271, 112898.
- Li, K., Chen, Y., Wang, M., Gong, A., 2019. Spatial-temporal variations of surface urban heat island intensity induced by different definitions of rural extents in China. *Sci. Total Environ.* 669, 229–247.
- Li, L., Zha, Y., Zhang, J., 2020a. Spatially non-stationary effect of underlying driving factors on surface urban heat islands in global major cities. *Int. J. Appl. Earth Obs. Geoinf.* 90, 102131.
- Li, X., Gong, P., Zhou, Y., Wang, J., Bai, Y., Chen, B., Hu, T., Xiao, Y., Xu, B., Yang, J., 2020b. Mapping global urban boundaries from the global artificial impervious area (GAIA) data. *Environ. Res. Lett.* 15, 094044.
- Li, X.-Y., 2003. Gravel-sand mulch for soil and water conservation in the semiarid loess region of Northwest China. *Catena* 52, 105–127.
- Liao, Y., Shen, X., Zhou, J., Ma, J., Zhang, X., Tang, W., Chen, Y., Ding, L., Wang, Z., 2022. Surface urban heat island detected by all-weather satellite land surface temperature. *Sci. Total Environ.* 811, 151405.
- Liu, H., He, B.-j., Gao, S., Zhan, Q., Yang, C., 2023. Influence of non-urban reference delineation on trend estimate of surface urban heat island intensity: a comparison of seven methods. *Remote Sens. Environ.*, 296, 113735.
- Liu, J., Schaaf, C., Strahler, A., Jiao, Z., Shuai, Y., Zhang, Q., Roman, M., Augustine, J., Dutton, E., Dutton, E., 2009. Validation of moderate resolution imaging Spectroradiometer (MODIS) albedo retrieval algorithm: dependence of albedo on solar zenith angle. *J. Geophys. Res. Atmos.* 114 (D1).
- Liu, Y., Huang, X., Yang, Q., Cao, Y., 2021. The turning point between urban vegetation and artificial surfaces for their competitive effect on land surface temperature. *J. Clean. Prod.* 292, 126034.
- Liu, Y., Zhang, X., Kong, X., Wang, R., Chen, L., 2018. Identifying the relationship between urban land expansion and human activities in the Yangtze River Economic Belt, China. *Appl. Geogr.* 94, 163–177.
- Liu, Z., Lai, J., Zhan, W., Bechtel, B., Voogt, J., Quan, J., Hu, L., Fu, P., Huang, F., Li, L., 2022a. Urban heat islands significantly reduced by COVID-19 lockdown. *Geophys. Res. Lett.* 49 e2021GL096842.
- Liu, Z., Zhan, W., Lai, J., Bechtel, B., Lee, X., Hong, F., Li, L., Huang, F., Li, J., 2022b. Taxonomy of seasonal and diurnal clear-sky climatology of surface urban heat island dynamics across global cities. *ISPRS J. Photogramm. Remote Sens.* 187, 14–33.
- Luo, Z., Asproudi, C., 2015. Subsurface urban heat island and its effects on horizontal ground-source heat pump potential under climate change. *Appl. Therm. Eng.* 90, 530–537.
- Mavrogianni, A., Davies, M., Batty, M., Belcher, S., Bohnenstengel, S., Carruthers, D., Chalabi, Z., Croxford, B., Demanuele, C., Evans, S., 2011. The comfort, energy and health implications of London's urban heat island. *Build. Serv. Eng. Res. Technol.* 32, 35–52.
- Miliaresis, G.C., Argialas, D., 1999. Segmentation of physiographic features from the global digital elevation model/GTOPO30. *Comput. Geosci.* 25, 715–728.
- Mohammad, P., Goswami, A., 2021. Quantifying diurnal and seasonal variation of surface urban heat island intensity and its associated determinants across different climatic zones over Indian cities. *GISci. Remote Sens.* 58, 955–981.

- Mohammad, P., Goswami, A., Bonafoni, S., 2019. The impact of the land cover dynamics on surface urban heat island variations in semi-arid cities: a case study in Ahmedabad City, India, using multi-sensor/source data. *Sensors* 19, 3701.
- Pekel, J.-F., Cottam, A., Gorelick, N., Belward, A.S., 2016. High-resolution mapping of global surface water and its long-term changes. *Nature* 540, 418–422.
- Peng, S., Piao, S., Ciais, P., Friedlingstein, P., Ottle, C., Bréon, F.-M., Nan, H., Zhou, L., Myneni, R.B., 2012. Surface urban heat island across 419 global big cities. *Environ. Sci. Technol.* 46, 696–703.
- Rasul, A., Balzter, H., Smith, C., 2016. Diurnal and seasonal variation of surface urban cool and heat islands in the semi-arid city of Erbil, Iraq. *Climate* 4, 42.
- Rasul, A., Balzter, H., Smith, C., Remedios, J., Adamu, B., Sobrino, J.A., Srivani, M., Weng, Q., 2017. A review on remote sensing of urban heat and cool islands. *Land* 6, 38.
- Reisi, M., Ahmadi Nadoushan, M., Aye, L., 2019. Remote sensing for urban heat and cool islands evaluation in semi-arid areas. *Glob. J. Environ. Sci. Manag.* 5, 319–330.
- Schwarz, N., Lautenbach, S., Seppelt, R., 2011. Exploring indicators for quantifying surface urban heat islands of European cities with MODIS land surface temperatures. *Remote Sens. Environ.* 115, 3175–3186.
- Sellers, P., Randall, D., Collatz, G., Berry, J., Field, C., Dazlich, D., Zhang, C., Collelo, G., Bounoua, L., 1996. A revised land surface parameterization (SIB2) for atmospheric GCMs. Part I: model formulation. *J. Clim.* 9, 676–705.
- Shafieiyoun, E., Gheysari, M., Khadiani, M., Abedi Koupai, J., 2023. Evaluating the spatiotemporal variations of daytime surface and canopy urban heat islands: an arid climate case study. *J. Environ. Plan. Manag.* 66, 2985–3006.
- Shen, Y., Chen, Y., 2010. Global perspective on hydrology, water balance, and water resources management in arid basins. *Hydrol. Process.* 24, 129–135.
- Shirani-Bidabadi, N., Nasrabadi, T., Faryadi, S., Larijani, A., Roodposhti, M.S., 2019. Evaluating the spatial distribution and the intensity of urban heat island using remote sensing, case study of Isfahan city in Iran. *Sustain. Cities Soc.* 45, 686–692.
- Siddiqui, A., Kushwaha, G., Nikam, B., Srivastav, S., Shelar, A., Kumar, P., 2021. Analysing the day/night seasonal and annual changes and trends in land surface temperature and surface urban heat island intensity (SUHII) for Indian cities. *Sustain. Cities Soc.* 75, 103374.
- Sofer, M., Potchter, O., 2006. The urban heat island of a city in an arid zone: the case of Eilat, Israel. *Theor. Appl. Climatol.* 85, 81–88.
- Streutker, D.R., 2002. A remote sensing study of the urban heat island of Houston, Texas. *Int. J. Remote Sens.* 23, 2595–2608.
- Sulla-Menashe, D., Friedl, M.A., 2018. User guide to collection 6 MODIS land cover (MCD12Q1 and MCD12C1) product. USGS: Reston, Va, USA 1, 18.
- Tran, H., Uchiyama, D., Ochi, S., Yasuoka, Y., 2006. Assessment with satellite data of the urban heat island effects in Asian mega cities. *Int. J. Appl. Earth Obs. Geoinf.* 8, 34–48.
- Tuholske, C., Caylor, K., Funk, C., Verdin, A., Sweeney, S., Grace, K., Peterson, P., Evans, T., 2021. Global urban population exposure to extreme heat. *Proc. Natl. Acad. Sci.* 118, e2024792118.
- Venter, Z.S., Chakraborty, T., Lee, X., 2021. Crowdsourced air temperatures contrast satellite measures of the urban heat island and its mechanisms. *Sci. Adv.* 7, eabb9569.
- Wan, Z., 2014. New refinements and validation of the collection-6 MODIS land-surface temperature/emissivity product. *Remote Sens. Environ.* 140, 36–45.
- Wang, J., Huang, B., Fu, D., Atkinson, P.M., 2015. Spatiotemporal variation in surface urban heat island intensity and associated determinants across major Chinese cities. *Remote Sens.* 7, 3670–3689.
- Wang, Q., Guan, Q., Lin, J., Luo, H., Tan, Z., Ma, Y., 2021. Simulating land use/land cover change in an arid region with the coupling models. *Ecol. Indic.* 122, 107231.
- Ward, K., Lauf, S., Kleinschmit, B., Endlicher, W., 2016. Heat waves and urban heat islands in Europe: a review of relevant drivers. *Sci. Total Environ.* 569, 527–539.
- Yang, C., Zhao, S., 2023. Diverse seasonal hysteresis of surface urban heat islands across Chinese cities: patterns and drivers. *Remote Sens. Environ.* 294, 113644.
- Yang, Q., Huang, X., Li, J., 2017. Assessing the relationship between surface urban heat islands and landscape patterns across climatic zones in China. *Sci. Rep.* 7, 9337.
- Yang, Q., Huang, X., Tang, Q., 2019. The footprint of urban heat island effect in 302 Chinese cities: temporal trends and associated factors. *Sci. Total Environ.* 655, 652–662.
- Yang, Q., Huang, X., Yang, J., Liu, Y., 2021. The relationship between land surface temperature and artificial impervious surface fraction in 682 global cities: spatiotemporal variations and drivers. *Environ. Res. Lett.* 16, 024032.
- Yang, Q., Xu, Y., Tong, X., Hu, T., Liu, Y., Chakraborty, T., Yao, R., Xiao, C., Chen, S., Ma, Z., 2023a. Influence of urban extent discrepancy on the estimation of surface urban heat island intensity: a global-scale assessment in 892 cities. *J. Clean. Prod.* 426, 139032.
- Yang, Q., Xu, Y., Tong, X., Huang, X., Liu, Y., Chakraborty, T.C., Xiao, C., Hu, T., 2023b. An adaptive synchronous extraction (ASE) method for estimating intensity and footprint of surface urban heat islands: a case study of 254 north American cities. *Remote Sens. Environ.* 297, 113777.
- Yang, Q., Xu, Y., Wen, D., Hu, T., Chakraborty, T., Liu, Y., Yao, R., Chen, S., Xiao, C., Yang, J., 2024. Satellite clear-sky observations overestimate surface urban heat islands in humid cities. *Geophys. Res. Lett.* 51 e2023GL106995.
- Yao, R., Huang, X., Zhang, Y., Wang, L., Li, J., Yang, Q., 2023. Estimation of the surface urban heat island intensity across 1031 global cities using the regression-modification-estimation (RME) method. *J. Clean. Prod.* 140231.
- Yao, R., Wang, L., Huang, X., Gong, W., Xia, X., 2019. Greening in rural areas increases the surface urban heat island intensity. *Geophys. Res. Lett.* 46, 2204–2212.
- Yao, R., Wang, L., Huang, X., Niu, Y., Chen, Y., Niu, Z., 2018. The influence of different data and method on estimating the surface urban heat island intensity. *Ecol. Indic.* 89, 45–55.
- Yao, R., Wang, L., Wang, S., Wang, L., Wei, J., Li, J., Yu, D., 2020. A detailed comparison of MYD11 and MYD21 land surface temperature products in mainland China. *Int. J. Digit. Earth.* 13, 1391–1407.
- Zandi, R., Salmani Moghadam, M., Roki, Z., 2023. Measuring the degree of spatial autocorrelation of land surface temperature with land use (Isfahan City). *Geogr. Environ. Plan.* 34, 61–76.
- Zhang, Z., Paschalidis, A., Mijic, A., Meili, N., Manoli, G., van Reeuwijk, M., Fatichi, S., 2022. A mechanistic assessment of urban heat island intensities and drivers across climates. *Urban Clim.* 44, 101215.
- Zhao, S., Zhou, D., Liu, S., 2016. Data concurrency is required for estimating urban heat island intensity. *Environ. Pollut.* 208, 118–124.
- Zhong, S., Qian, Y., Zhao, C., Leung, R., Wang, H., Yang, B., Fan, J., Yan, H., Yang, X.-Q., Liu, D., 2017. Urbanization-induced urban heat island and aerosol effects on climate extremes in the Yangtze River Delta region of China. *Atmos. Chem. Phys.* 17, 5439–5457.
- Zhou, D., Xiao, J., Bonafoni, S., Berger, C., Deilami, K., Zhou, Y., Froliking, S., Yao, R., Qiao, Z., Sobrino, J.A., 2018. Satellite remote sensing of surface urban heat islands: Progress, challenges, and perspectives. *Remote Sens.* 11, 48.
- Zhou, D., Zhao, S., Liu, S., Zhang, L., Zhu, C., 2014. Surface urban heat island in China's 32 major cities: spatial patterns and drivers. *Remote Sens. Environ.* 152, 51–61.
- Zhou, J., Li, J., Yue, J., 2010. Analysis of urban heat island (UHI) in the Beijing metropolitan area by time-series MODIS data. In: In, 2010 IEEE International Geoscience and Remote Sensing Symposium. IEEE, pp. 3327–3330.